Dynamics of inhibitory networks in the Olfactory Bulb

A THESIS SUBMITTED

IN PARTIAL FULFILLMENT OF THE

REQUIREMENTS FOR THE DEGREE OF

DOCTOR OF PHILOSOPHY

BY

SHIVIK GARG

20133247

IISER PUNE

INDIAN INSTITUTE OF SCIENCE EDUCATION

AND RESEARCH, PUNE

2019

CERTIFICATE

Certified that the work incorporated in the thesis entitled **"Dynamics of inhibitory networks in the Olfactory Bulb"**, submitted by Mr. Shivik Garg was carried out by the candidate, under my supervision. The work presented here or any part of it has not been included in any other thesis submitted previously for the award of any degree or diploma from any other university or institution.

Dr. Collins Assisi

Supervisor

12/06/19
Date

DECLARATION

I, declare that this written submission represents my ideas in my own words, and where other's ideas have been included, I have adequately cited and referenced the original sources. I also declare that I have adhered to all principles of academic honesty and integrity and have not misrepresented or fabricated or falsified any idea/data/fact/source in my submission. I understand that violation of the above will be cause for disciplinary action by the Institute and can also evoke penal action from the sources which have thus not been properly cited or from whom proper permission has not been taken when needed.

Shivik Garg

Reg. No. 20133247

Date: 15/06/2019

To, my late brother CA Shaurya Garg,

for his encouragement and motivation.

ACKNOWLEDGEMENTS

Ph.D. is a long arduous journey filled with lots of ups and downs. Although this thesis bears my name but there were a lot of people without whose support and contributions I would not have been able to reach the finish line. It gives me great pleasure to acknowledge and extend a note of gratitude for their support.

First and foremost I would like to thank Dr. Collins Assisi my thesis supervisor for his support, encouragement, patience and guidance. His insights and suggestions helped me in shaping the project. He gave me the freedom to explore things which helped me gain experience in the field of computational neuroscience. His mentoring helped in learning about how to address the scientific problems.

I am grateful to my Research advisory committee members Dr. Aurnab Ghose, Dr. Nixon Abraham and Dr. Raghav Rajan for their support and comments regarding my research work.

I would like to thank Dr. Suhita Nadkarni and her lab members for their comments and suggestions regarding the work. I would like to thank Rohan with whom I discussed not only about my project but also about our alma mater IIT Kanpur and various other topics ranging from sports to politics.

Special thanks to my labmate Arun Neru for patiently listening to my problems and helping me out in understanding some of the concepts in this field. Discussions with him about my project helped me clear some of the doubts and I was able to make good progress. I will never forget our discussions our tea sessions over which we discussed a lot.

I am grateful to Pranav for designing insilico without which I would not have been able to do the simulations. I also want to thank Divye for his help in analyzing the data.

During my time at IISER I was able to make friendship with lot of people on and off the sporting field. Big shout out to Mahesh, Ravi, Jay Prakash, Ishtiyaq, Neelesh and all those people with whom I played different sports and was fortunate to be able to enjoy some downtime away from the stress of Ph.D life.

I would also like to thank my friends outside IISER Krishna, Dilip, Deepak, Vikrant, Sarojini, Aditi, Saurabh, Pradipt for their support during my tough times.

TABLE OF CONTENTS

List of Abbreviations

2-DG: 2-deoxy-D-glucose

AB: Anterior Burster Neuron

AHP: Afterhyperpolarization

AL: Antennal Lobe

AMPA: α-amino-3-hydroxy-5-methyl-4-isoxazoepropionic acid

BOLD fMRI: Blood oxygen level dependent fMRI

CNG: Cyclic-nucleotide gated channel

CPG: Central Pattern Generator

DTI: Diffusion Tensor Imaging

EEG: Electroencephalography

EPL: External Plexiform Layer

ET: External Tufted Cells

fMRI: Functional Magnetic Resonance Imaging

GABA: γ-aminobuytric acid

GCL: Granule Cell Layer

GL: Glomerular Layer

IPL: Internal Plexiform Layer

IPSC: Inhibitory post synaptic current

JG: Juxtaglomerular Cells

LFP: Local Field Potential

LN: Local Neurons

LOT: Lateral Olfactory Tract

MCL: Mitral Cell Layer

MEG: Magnetoencelphalography

NMDA: N-methyl-D-aspartate

OB: Olfactory Bulb

ODE: Ordinary Differential Equation

ONL: Olfactory Nerve Layer

OR: Olfactory Receptor

ORN: Olfactory Receptor Neuron

PD: Pyloric Dilator

PG: Periglomerular Cells

PN: Principal Neurons

rsFC: resting state functional connectivity

sSA: Short axon cells

STO: Subthreshold Oscillation

WLC: Winnerless Competition

List of Figures

Synopsis

Dynamics of Inhibitory Networks in Olfactory Bulb

Name: Shivik Rakesh Garg

Roll Number: 20133247

Name of Supervisor: Dr. Collins Assisi

Department: Biology, IISER Pune

Date of Registration: 22nd January, 2013

Chapter 1 Introduction

Sensory systems are involved in creating an internal representation of the external world which helps the animal to produce an appropriate behavioral response. The olfactory system is involved in detecting and processing various volatile chemical compounds. The mammalian olfactory system is organized into three different layers namely; olfactory receptor neurons, olfactory bulb and olfactory cortex **(Shepherd and Greer, 2004)**. Odor detection begins when odor molecules bind to the G-protein coupled receptors present on the olfactory receptor neurons (ORNs). It was discovered that the olfactory system expresses a vast repertoire of odorant receptors (ORs) and the tuning properties of these ORs vary: some are broadly tuned whereas some are narrowly tuned and thus odors are encoded in a combinatorial fashion by the ORNs **(Axel, 1995; Hallem and Carlson, 2006)**. This helps in recognizing a diverse array of odor molecules. Odor binding depolarizes the ORNs and this information is then sent to the olfactory bulb where the ORNs innervate spherical structures known as glomeruli. Each glomeruli in the bulb is homogeneous, meaning all the ORNs that innervate a particular glomerulus express the same OR. Within the glomeruli the mitral cells make synaptic connections with the ORNs. The mitral cells are coupled to each other through inhibitory interneurons known as granule cells. Based on this wiring patterns of ORNs it has been proposed that in the bulb also combinatorial coding of odors takes place. However studies done in locust antennal lobe as well as zebrafish olfactory bulb have shown that odors are represented as spatiotemporal patterns of activity of the principal neurons characterized by epochs of inhibition

and excitation **(Friedrich and Laurent, 2001; Laurent and Davidowitz, 1994; Laurent et al., 1996)**. Inhibition plays an important role in organizing these spatiotemporal patterns of activity, as blocking inhibition through GABA antagonist causes desynchronization of PNs and leads to impairment in odor discrimination **(Stopfer et al., 1997)**. In the bulb inhibition from granule cells has been shown to generate synchronized firing in the mitral cells **(Schoppa, 2006)**. Apart from inhibition, the underlying structure of the network also governs the generation of these patterns. Studies of simple microcircuits such as central pattern generators have helped in understanding dynamics in larger complex networks. CPGs mostly consist of neurons which are connected to each other through reciprocal inhibition and generate rhythmic motor movement **(Marder and Bucher, 2001, 2007)**. Earlier work has shown that graph coloring can be used to study the relationship between inhibitory networks and their dynamics **(Assisi et al., 2011)**. While this relationship is easy to observe for small or regular networks, it is not possible to obtain all possible colorings for complex topologies in a reasonable period of time. Brain connectomic studies, which involve applying graph theory techniques to study the organizational features of anatomical connections across cortical structures found that these networks are modular in nature **(Sporns, 2013)**. Computational modeling shows that synchronization dynamics in these networks is shaped by the underlying structure. These networks consist of neurons which are coupled to each other through excitatory connections. In our study, to overcome the limitation of graph coloring, we used community clustering algorithm to study the relationship between modularity of inhibitory networks and their dynamics. Modularity for inhibitory networks is defined as group of neurons that are maximally disconnected from each other but connected among other groups.

Chapter 2 Spatiotemporal Patterning in Mitral Cell Network

We simplified the bulb circuitry as an inhibitory network of mitral cells. In our simulations upon injection of depolarizing current to mitral cells show clustered action potentials interspersed with subthreshold oscillations (STOs). The clustering of spikes arises because of the slow potassium current and the STOs because of the interaction of slow potassium and persistent sodium. Our simulations show that when mitral cells are coupled to each other through lateral inhibition it results in switching of activity in the mitral cells. To investigate what factors contribute to sequential activity in the mitral cells we simulated a random motif of six mitral cells. On

simulating this network, we see temporal ordering in the firing of mitral cells with certain neurons firing together and other neurons firing synchronously at different times. The inactivation variable of the slow potassium current determines which neuron fires next in the sequence.

Chapter 3 Correlation between dynamics and inhibitory network structure

In the olfactory bulb different odors activate different subnetworks and therefore we simulated random inhibitory subnetworks of the mitral cells. In an inhibitory network, neurons that inhibit each other form groups that fire at different times. We used Newman clustering algorithm to cluster our inhibitory subnetworks and tried to find groups of neurons that will fire synchronously forming a spatiotemporal pattern. This algorithm tries to find communities based on edge densities such that the resulting communities should have higher edge densities within the communities and sparser across communities. This is done using a measure known as the modularity. Since our networks are inhibitory we used the flipped version of the adjacency matrix to find such groups. Upon clustering we permuted the original matrix to reveal such groups having minimum within group connections. Upon simulating such random networks we were able to extract hidden correlations between network structure and the dynamics. The clusters identified helped in revealing groups of neurons that fired synchronously but did not specify the temporal ordering. We simulated different instances of random networks and using our method we were able to extract such communities for different random networks. These correlations persisted across different noise trials. We then tried a different approach in which using the dynamics we tried to cluster the activity of neurons using spike synchronization measure and k-medoid clustering. We were able to find groups of neurons that fired synchronously revealing the spatiotemporal dynamics. We also found good overlap between the dynamics based clustering and the structure based clustering.

Chapter 4 Asymmetries and Reliability in dynamics

In the locust antennal lobe PNs response to odor stimulus is reliable across different noise trials. Similar observation has been recorded in the mitral cells of zebrafish. We investigated how network topology can help in inducing reliability in the patterns across noise perturbations. Theoretical work using simpler and smaller networks have shown that asymmetry in network

conditions can induce reliability across noise trials. Based on this work we simulated mitral cell network of 40 neurons with symmetry in network connections and found that they generated different temporal orderings across noise trials making it unreliable. When we introduced asymmetry in the network by making preferential connections from one group to another, we found that the ordering of the dynamics becomes reliable across noise trials. We quantify reliability using an entropy measure. For reliable patterns entropy value is close to zero. We find that in case of symmetric network the entropy value is high whereas in asymmetric cases entropy value is close to zero.

To summarize, using Newman clustering algorithm we were able to extract hidden correlations between network topology and dynamics. The algorithm found neurons that fired synchronously but the temporal ordering was not specified. These correlations persisted across different noise trials, but they generated different ordering in each trial making it unreliable. Asymmetries in network topology induced a particular ordering in the patterns that was reliable across noise trials. The work shows that lateral inhibition in the bulb plays a role in generating spatiotemporal patterning, and we speculate that this would help in decorrelating patterns evoked by similar odor pairs. Our work has implications in further studying the olfactory bulb dynamics such as the possible role of sniff cycle in inducing reliability in mitral cell spiking. Also our method can be used for studying brain regions where inhibitory networks are involved in information processing.

REFERENCES

Assisi, C., Stopfer, M., and Bazhenov, M. (2011). Using the structure of inhibitory networks to unravel mechanisms of spatiotemporal patterning. Neuron *69*, 373-386.

Axel, R. (1995). The molecular logic of smell. Sci Am *273*, 154-159.

Friedrich, R.W., and Laurent, G. (2001). Dynamic optimization of odor representations by slow temporal patterning of mitral cell activity. Science *291*, 889-894.

Hallem, E.A., and Carlson, J.R. (2006). Coding of odors by a receptor repertoire. Cell *125*, 143-160.

Laurent, G., and Davidowitz, H. (1994). Encoding of olfactory information with oscillating neural assemblies. Science *265*, 1872-1875.

Laurent, G., Wehr, M., and Davidowitz, H. (1996). Temporal representations of odors in an olfactory network. J Neurosci *16*, 3837-3847.

Marder, E., and Bucher, D. (2001). Central pattern generators and the control of rhythmic movements. Curr Biol *11*, R986-996.

Marder, E., and Bucher, D. (2007). Understanding circuit dynamics using the stomatogastric nervous system of lobsters and crabs. Annu Rev Physiol *69*, 291-316.

Schoppa, N.E. (2006). Synchronization of olfactory bulb mitral cells by precisely timed inhibitory inputs. Neuron *49*, 271-283.

Shepherd, G.M., and Greer, C.A. (2004). Olfactory Bulb. In Synaptic organization of the brain (New York,NY: Oxford University Press), pp. 165-216.

Sporns, O. (2013). Structure and function of complex brain networks. Dialogues in clinical neuroscience *15*, 247-262.

Stopfer, M., Bhagavan, S., Smith, B.H., and Laurent, G. (1997). Impaired odour discrimination on desynchronization of odour-encoding neural assemblies. Nature *390*, 70-74.

Chapter 1: Introduction

1.1 Introduction

Sensory systems are involved in creating an internal representation of the external world which help the animal to produce an appropriate behavioral response. The olfactory system detects and processes various volatile chemical compounds. The olfactory system has a great ability to recognize a diverse range of odor molecules which are helpful for animals in locating the source of food, identifying conspecifics, avoiding predators, finding partners for reproduction and avoiding death. Olfactory system, like the visual and auditory system can detect and discriminate between a wide range of stimuli. However, odors are characterized by a multidimensional chemical space, unlike visual and auditory stimuli, which can be classified by a single parameter like wavelength and frequency respectively (**Su et al., 2009**). The olfactory system in addition to recognition also helps the animal in discriminating between a variety of odor molecules. Representations of certain odor molecules are learned and stored as memory for future recall. The underlying olfactory circuitry plays an important role in performing these diverse functions of recognition, discrimination and learning.

There are striking similarities in the way the olfactory system is organized across different animal species. These include presence of receptor neurons for odor detection, a second messenger signaling pathway and convergence of particular receptor neurons to neurophil structures known as glomeruli. It has been proposed that these similarities have occurred due to convergent evolution of the olfactory system and point to an optimal solution to the problem of odor detection and discrimination (**Ache and Young, 2005; Eisthen, 2002**). Despite these similarities, certain differences do exist. The olfactory bulb in mammals is a highly laminated structure comprising of two different populations of principal neurons namely mitral and tufted cells. There are a large number of different interneuron populations present in the bulb. The bulb principal neurons project to the olfactory cortex which sends feedback connections to the bulb. The insect antennal lobe, which is analogous to the olfactory bulb, is not highly layered like it. The excitatory population in the lobe are the principal neurons and the inhibitory population are the local interneurons. PNs send projections to the mushroom body (MB) (MB is analogous to the olfactory cortex) and the MB sends feedback to the antennal lobe (**Ache and Young, 2005; Eisthen, 2002; Hildebrand and Shepherd, 1997; Hu et al., 2010; Rybak and Menzel, 1993**). Since the overall functional

organization of the olfactory system is similar across species, fundamental insights gained from a particular organism can be equally applied to others.

We are interested in studying how the olfactory system encodes odors as spatiotemporal patterns. These patterns arise because of the input to the bulb from the ORNs and the network architecture of the bulb. The following section describes the anatomical features of the olfactory system to understand how information flows across different layers before being finally sent to the olfactory cortex.

1.2 Anatomy of the Olfactory System

1.2.1 Olfactory Receptor Neurons

Olfactory receptor neurons (ORNs) represent the first level of processing in the olfactory system. ORNs are bipolar neurons lining up the nasal epithelium. The apical side of the ORNs projects a single dendrite into the mucosal covering of the epithelium. The dendrite ends up into a knob-like structure from which 20-30 cilia emerge **(Firestein, 2001)**. On the proximal side an unmyelinated axon projects into the olfactory bulb **(Buck, 1996; Mombaerts, 1999)**. How are odors detected by this first layer? Volatile odorant molecules enter the nasal cavity and bind to the odorant receptors (ORs) present on the cilia of the ORNs. The odorant receptors belong to the G-protein receptor family and consist of a seven-transmembrane domain (7TD) **(Touhara and Vosshall, 2009)**. Binding of the odorant molecules to the G-protein coupled receptors initiates adenylyl cyclase/cAMP second messenger cascade system leading to the opening of cyclic-nucleotide gated channel (CNG). Opening of the CNG channels leads to an influx of Ca^{2+} and to some extent Na^+ ions into the membrane. This influx of Ca^{2+} causes depolarization of the ORNs which is amplified because of the efflux of Cl^- through Ca^{2+} activated chloride channel **(Lowe and Gold, 1993; Restrepo et al., 1996)**. The depolarization initiated in the cilia leads to the generation of action potentials at the soma which propagates along the axon and the signal is transmitted to the olfactory bulb. Thus the ORNs are involved in transduction of chemical stimulus into an electrical stimulus.

Identification of different odorant receptors and the wiring of the ORNs in the olfactory bulb helped in deciphering the molecular mechanism underlying odor detection **(Axel, 1995)**. Pioneering work done in 1991 led to the discovery that ORs are coded by a large multigene family and each ORN expresses only one particular type of odorant receptor **(Buck and Axel, 1991)**. The

total number of odorant receptors expressed in each species varies. There are about 1000 different types of receptors found in the mice olfactory system, in zebrafish the number of ORs is about 140, 160 in honeybees and around 400 in humans **(Alioto and Ngai, 2005; Go and Niimura, 2008; Robertson and Wanner, 2006; Zhang and Firestein, 2002)**. The presence of a large number of different ORs endows the olfactory system with the ability to detect and discriminate a large set of odor molecules. All the ORNs that express a particular OR converge to one or two glomeruli in the olfactory bulb **(Mombaerts, 1999; Vassar et al., 1993)**.

1.2.2   Olfactory Bulb

Olfactory bulb is the next relay layer after ORNs in the olfactory system. The Olfactory bulb is a laminar structure comprising of multiple layers (Figure 1.1). The five prominent layers of the bulb from superficial to deep layers are: glomerular layer (GL), External Plexiform Layer (EPL), Mitral Cell Layer (MCL), Internal Plexiform Layer (IPL) and the Granule Cell Layer (GCL). The glomerular layer consists of glomeruli which are well-defined spherical neurophil structures. The ORNs get bundled together into the olfactory nerve and after reaching the bulb defasciculate and innervate the appropriate target glomerulus. Each glomerulus receives thousands of ORNs all of which express the same OR. This has come to be known as the glomerular convergence rule. The number of glomeruli varies in each species. There are about 1800 glomeruli in the mouse, 4200 in the rat and 6300 in rabbit **(Royet et al., 1998).** The size of the glomeruli also varies according to the species. They are around 20-40 μm in diameter in fish and amphibians and do not have clear boundaries. In mice they are about 30-50 μm in diameter whereas in rabbit they are around 100-200 μm **(Shepherd and Greer, 2004).** The neurons found within or surrounding the glomeruli are collectively known as juxtaglomerular cells (JG). Three morphologically distinct neuronal populations comprise the JG cells. They are the periglomerular cells (PG), External Tufted Cells (ET) and the superficial short axon cells (sSA) **(Nagayama et al., 2014; Pinching and Powell, 1971a, b, c)**. PG cells are involved in modulating the activity of a particular glomerular unit. The dendrites of the PG cells are localized within a single glomerulus forming intraglomerular connections. They receive excitatory inputs from the ORNs via the axodendritic synapses and also from the mitral/tufted cells via the dendrodendritic synapses. PG cells mediate inhibition onto the mitral/tufted cells by releasing GABA and thus shape their activity patterns. Axons of the sSA

cells span multiple glomeruli forming interglomerular connections. In contrast to PG cells they release glutamatergic neurotransmitter and their function is not well known **(Yamaguchi, 2014)**. The principal neurons of the bulb, namely the tufted and mitral cells, project their primary dendrite into a single glomerulus where it branches into a tuft like structure. They make axodendritic synaptic contacts with the ORNs. The mitral/tufted cells also give rise to the secondary dendrites (also known as lateral dendrites) and these are found in the EPL. These secondary dendrites are 1-6µm in diameter and can extend upto 1mm in length. The cell body of the tufted cells is located in the EPL whereas that of the mitral cell is found in the MCL which is around 200-400 µm deep to the GL. The axons of the mitral cells and tufted cells are found in the IPL. The granule cell layer (GCL), which lies beneath the IPL, contains the soma of the granule cells. The cell bodies of granule cells are small and have a diameter of 6-8µm. Granule cells have an apical dendrite which extends into the EPL and a basal dendrite located in the GCL, however they lack an axon. Granule cells are GABAergic neurons and are the primary inhibitory interneurons of the bulb. Unlike most brain regions the inhibitory population outnumbers the excitatory population in the olfactory bulb. The granule cell dendrites contain a large number of spines which are also known as gemmules. The apical dendrites of the granule cells make reciprocal dendrodendritic connections with the lateral dendrites of the mitral/tufted cells. This dendrodendritic synapse is the hallmark of the olfactory bulb. A particular granule cell makes synaptic contacts with mitral cells belonging to the same glomerular unit as well as mitral cells belonging to another glomerular unit and thus facilitating recurrent as well as lateral inhibition. Action potentials generated in the mitral cells back propagate into the lateral dendrites and depolarize them causing release of glutamate. Glutamate release activates the NMDA and AMPA receptors present on the gemmules of granule cell spines. This leads to depolarization of granule cells. This depolarization causes activation of calcium gated channels leading to an influx of calcium which then facilitates the release of GABA. The GABA then binds to the receptors present on the lateral dendrites of mitral cells mediating lateral as well as recurrent inhibition of the mitral cells (Figure 1.2) **(Shepherd and Greer, 2004)**.
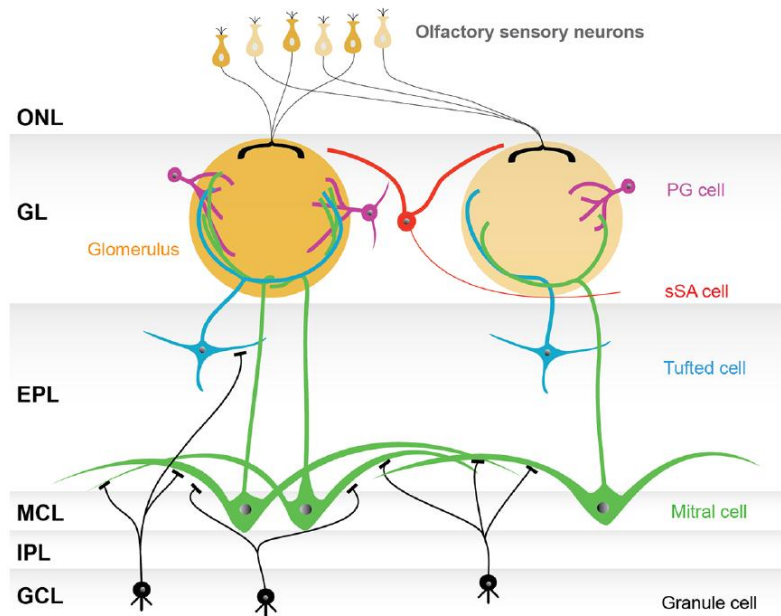
Figure 1.1 Diagram showing the connectivity in the olfactory bulb

Mitral (red) and Tufted (blue) cells send projections to the glomerulus where they make synaptic contacts with the ORNs. Mitral/tufted cells also make reciprocal dendrodendritic connections with the granule cells. Reproduced from (Nagayama et al., 2014) with permission.
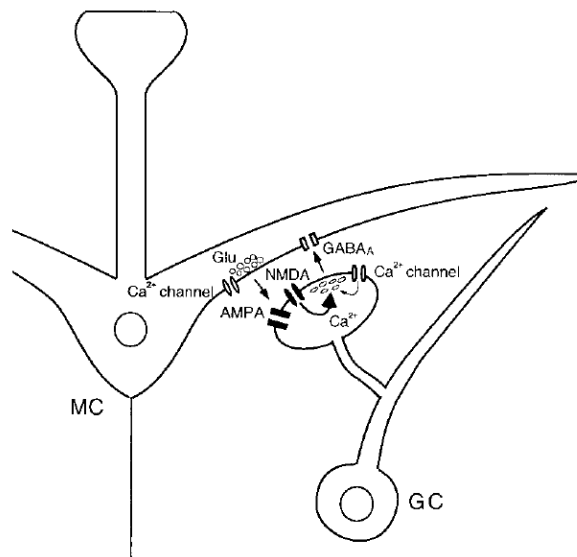
Figure 1.2 Diagram showing the dendrodendritic synapse between mitral cell lateral dendrite and the granule cell apical dendrite

Mitral cell lateral dendrite upon activation releases glutamate which excites the granule cells via AMPA and NMDA receptors. This leads to release of GABA onto the mitral cell dendrite by the granule cells. Reproduced from (Chen et al., 2000) with permission.

1.2.3 Olfactory Cortex

The olfactory cortex is made up of those regions that receive direct innervations from the olfactory bulb projection neurons. These include piriform cortex (anterior and posterior piriform cortex), olfactory tubercle, cortical areas of olfactory peduncle (anterior olfactory cortex, tenia tecta, and dorsal peduncular cortex), cortical amygdaloid nuclei (nucleus of the lateral olfactory tract, anterior cortical amygdaloid nucleus and posterior cortical amygdaloid nucleus) and lateral entorhinal cortex **(Haberly and Price, 1977; Mori and Manabe, 2014; Neville and Haberly, 2004; Price, 1973).** As compared to other sensory systems input to the cortex does not arrive via relay to the thalamus. The olfactory cortex is a laminar structure comprising of three layers instead of the usual six layers found in the neocortex. One of the extensively studied regions of the olfactory cortex is the piriform cortex. The entire piriform cortex has the same organizational features and it consists of three distinct layers namely Layer I, II and III. Layer I is subdivided into a superficial layer Ia which receives afferent input from the bulb via the lateral olfactory tract (LOT) and a deep layer Ib which receives connections from other areas of the olfactory cortex. Similarly, Layer II has a superficial layer known as IIa which consists of semilunar cells and a deep layer IIb which contains cell bodies of superficial pyramidal cells. Layer III consists of deep pyramidal cells. Layer II and Layer III pyramidal cells are considered as the principal cells of the olfactory cortex because they have large dendritic trees and they project their axons to a large number of different areas. Pyramidal cells of Layer II and Layer III cannot be differentiated from each other morphologically. Deeper to Layer III is another layer known as the endopiriform nucleus **(Mori and Manabe, 2014; Neville and Haberly, 2004)**. Pyramidal cells of the piriform cortex as well as other olfactory cortical areas send large amounts of axon collaterals (centrifugal inputs) back to the olfactory bulb forming a top-down feedback pathway **(de Olmos et al., 1978)**. These axonal collaterals project heavily to the GCL and the granule cells are the primary recipients of these connections. They also make sparser connections with deep short axon cells found in the GCL. The centrifugal connections mediate disynaptic feedforward inhibition of the mitral cells through AMPA receptors present on the granule cells **(Boyd et al., 2012; de Olmos et al., 1978)**. Experimental studies suggest that feedback centrifugal connections play a role in olfactory learning **(Gao and Strowbridge, 2009; Gschwend et al., 2015)**

Odor recognition begins at the ORN level and undergoes transformations at each level before the information is sent to the olfactory cortex. Below we focus on odor representation in the olfactory bulb.

1.3 Encoding of odors (representations)

1.3.1 Representation of Odors by ORNs

Odor perception begins when odorant molecules bind to the odorant receptors initiating second messenger cascade signaling. Discovery of the presence of large repertoire of odorant receptors led to the suggestion that odors are encoded as preferential responses of some ORs **(Axel, 1995; Buck, 1996)**. Later studies showed that OR responses to odorant molecules are either excitatory or inhibitory and they are differentially tuned. Some ORs respond to a large number of odor molecules and are hence referred to as being broadly tuned. On the other hand, some respond to only a narrow set of molecules and are referred to as being narrowly tuned. The breadth of the tuning reveals the discriminatory power of the odorant receptor. These studies also showed that a single odorant stimulus can activate multiple odorant receptors. This diversity in the response properties of ORNs enables the system to implement an elaborate combinatorial encoding of a wide array of odors **(Hallem and Carlson, 2006).** Studies done in locusts reveal that ORN's responses to odors are temporally heterogeneous; which is characterized by latency in spiking, onset and offset time, rate of adaptation and peak amplitude. The different temporal properties of ORN firing are believed to contain information about odor identity, concentration and duration of the odor presented. Complex spatiotemporal patterns were generated by the AL when there was heterogeneity in the duration of ORN response time as well as its amplitude **(Raman et al., 2010)**. However, the temporal complexity of the antennal lobe is far more dynamic than what is observed for the ORNs.

1.3.2 Spatial Coding of Odors in the Olfactory Bulb

The ORNs, after transduction of the chemical information of odorant molecule into an electrical stimulus, send this information to the olfactory bulb glomeruli. It has been long thought that odor encoding in the olfactory bulb occurs in a combinatorial manner. It has been proposed that different odors will activate different and distinct spatial patterns of glomeurli. Thus, transformation of odor

information encoded by the ORNs to the activation of glomerular patterns in the olfactory bulb has been studied using various approaches. Initial studies were done based on uptake of radioactively labeled [^{14}C] 2-deoxy-D-glucose (2-DG) to map the sites of activation in the glomerulus. The rats were injected with radioactive 2-DG and exposed to amyl acetate. The glomeruli that were activated by this odor, increased their 2-DG uptake which was reflected in the increased intensity on autoradiographs. Further studies done using 2-DG uptake showed that different odors activated different foci of glomeruli, thus providing evidence for a spatial coding scheme in the bulb (**Jourdan et al., 1980; Sharp et al., 1975; Stewart et al., 1979**). Guthrie et. al. used a marker, known as immediate early gene *c-fos* expression, to study odorant evoked neuronal activity and found that it confirmed the studies of 2-DG uptake that odors activate focal patterns in the glomeruli (**Guthrie et al., 1993**). Optical imaging of the olfactory bulb using Ca^{2+} sensitive dyes in the ORNs indicate that different odorants evoke different combinations of glomeruli and similar odors evoke overlapping but distinct spatial patterns of glomeruli (**Friedrich and Korsching, 1997, 1998**). Optical imaging using intrinsic signals have also reached similar conclusions (**Rubin and Katz, 1999**). Other techniques such as fMRI and 2 photon Ca^{2+} imaging also show that odorants evoke specific spatial patterns of activity in the glomeruli (**Wachowiak and Cohen, 2001; Yang et al., 1998**). In a study done with large number of different enantiomer pairs, it was found that rats readily discriminated between them. Optical imaging revealed that the enantiomer pairs activated distinct spatial glomeruli patterns in the bulb, thus providing support that spatial activity pattern contains sufficient information to create distinct identities which helps in odor discrimination (**Rubin and Katz, 2001**). Thus these experimental studies have shown that odors evoke spatial patterns of glomerular activation and that a combinatorial coding scheme of odor processing occurs in the olfactory bulb. A recent study has also supported this argument where they show that the olfactory bulb circuitry is involved in linearly summating the input received from the ORNs (**Gupta et al., 2015**).

1.3.3 Spatio-Temporal Coding in the Olfactory Bulb

Studies regarding odor encoding suggest that in addition to the spatial dimension, the temporal dimension also plays an important role in odor stimulus processing. The role of time in olfactory coding comes with respect to observations such as the presence of oscillatory activity in the

olfactory bulb. Odor evoked oscillations in the local field potential recordings of the mammalian olfactory bulb were first revealed by **E.D. Adrian (Adrian, 1942).** The sine wave like oscillatory activity was found to be in the frequency range of 35-80 Hz **(Bressler and Freeman, 1980)**. Early computational models suggested that temporal patterning in mitral cell spiking activity may play a role in odor processing **(Meredith, 1992; Schild, 1988).** Recordings in the rabbit olfactory bulb showed that mitral/tufted cell spike discharges have a temporal relationship with the oscillatory LFP. This showed that the rhythmic oscillatory drive occurs due to the synchronized activity of the mitral/tufted cells **(Kashiwadani et al., 1999).** Experiments done using voltage sensitive dye imaging in the rodent olfactory bulb have also shown that odors evoke spatio-temporal patterns of activity **(Spors and Grinvald, 2002)**. Mitral cells of zebrafish olfactory bulb respond to odors with complex spatiotemporal patterns that evolve over hundreds of milliseconds, consisting of epochs of excitation and inhibition **(Friedrich and Laurent, 2001)**. Similar slow temporal patterns have also been observed in the antennal lobe of locusts **(Laurent et al., 1996a; Wehr and Laurent, 1996).** Odor evoked oscillatory activity has been observed in the antennal lobe and the antennal lobe circuitry itself generates these odor evoked oscillatory activity, as ablation of the mushroom body did not result in ablation of the oscillatory activity in the AL **(Laurent and Davidowitz, 1994)**. It has been shown that blocking of synchronization in honeybee antennal lobe leads to loss of odor discrimination between similar pair of odors suggesting that oscillatory synchronization of PNs plays an essential role in odor processing **(Stopfer et al., 1997)**. Laurent has proposed a coding scheme whereby the antennal lobe circuitry using the spatiotemporal patterns of activity expands the coding capacity of the olfactory system. These slow temporal patterns of activity evolve along the oscillatory LFP with different groups of principal neurons getting entrained at each cycle of the oscillation **(Laurent, 2002)**. It has been proposed that this slow temporal patterning helps in reducing the overlap between representations of similar odors helping in decorrelation and discrimination. Inhibition from local interneurons has been shown to play an important role in generating the precise spiking patterns of principal neurons in the honeybee antennal lobe **(Stopfer et al., 1997)**.

1.4 Role of Inhibition

The olfactory bulb contains a large number of inhibitory interneurons which outnumber the excitatory neurons (mitral/tufted cells) and thus inhibition plays a key role in shaping and regulating the mitral/tufted cell activity. There are various roles that have been attributed to inhibition:

1.4.1   Oscillatory Activity and Slow Temporal Patterning

It has been found that the circuitry of the insect antennal lobe generates oscillatory activity. Blocking inhibition on to the principal neurons (PNs) by applying $GABA_A$ antagonist picrotoxin in the antennal lobe abolishes the oscillations as seen in the local field potential recordings while leaving the slow patterns unaffected, thus showing that inhibition plays a role in shaping the patterns of principal neurons (**MacLeod and Laurent, 1996**). Applying $GABA_B$ antagonist has been found to abolish these slow temporal patterns (**Wilson and Laurent, 2005**). Similarly applying picrotoxin in the honeybee antennal lobe abolishes the 30Hz oscillatory activity and also leads to loss of precise firing of the PNs causing impairment in odor discrimination (**Stopfer et al., 1997**). These studies show that inhibition plays an important role in organizing these spatiotemporal patterns. It has been shown that inhibitory interactions in the LN subnetwork entrains different populations of PN which participate in forming spatiotemporal patterns (**Bazhenov et al., 2001**). Similarly in another computational study it has been shown how the inhibitory subnetwork of the LN population shapes the spatiotemporal patterns of activity(**Assisi et al., 2011**). Theoretical work done using simpler models have shown that inhibitory networks generate dynamics through competition, known as winnerless competition (WLC) and it has proposed that the spatiotemporal patterns of odors resemble these dynamics (**Rabinovich et al., 2001**). In the olfactory bulb reciprocal dendrodendritic synapses mediate synchronization of the mitral cells. Synchronized feedback inhibition from granule cells onto the mitral cells shapes their spike times leading to the synchronized oscillatory activity and generating the characteristic 40 Hz oscillations (**Lagier et al., 2004; Schoppa, 2006**). A computational study has shown how inhibition along with subthreshold oscillations play a role in generating the gamma oscillations in the mitral cell population (**Brea et al., 2009**). Psychophysical studies have shown that increasing inhibition on to the mitral cells leads to faster discrimination ability of mice for similar odor pairs.

This suggests inhibition plays a role in organizing spatiotemporal patterns of activity for odors (**Abraham et al., 2010**).

1.4.2 Contrast Enhancement

Another role that has been attributed to inhibition in the olfactory system is the role of contrast enhancement. Contrast enhancement has been studied in case of the visual system, where it helps in improving the spatial contrast between light and dark regions. Contrast enhancement occurs by lateral inhibition and it involves sharpening of neural representations by inhibiting nearby neurons and thus enhancing the difference between stimulus and the background (**Cleland and Linster, 2005**). Investigators have explored whether similar phenomenon takes place in the olfactory bulb They have argued that lateral inhibition in the bulb is facilitated by the lateral dendrites of the mitral cells. The most direct evidence for contrast enhancement in the bulb came from the studies of Yokoi et. al. in 1995. Using single unit recordings of mitral/tufted cells, their response to a series of aliphatic aldehydes consisting of increasing carbon chain length was recorded. It was found that mitral cells can respond to a wide range of related odors but receive lateral inhibition from flanking mitral cells. The weaker responses to an odor were inhibited by strong lateral inhibition. This led to the sharpening of responses to a defined set of odor molecules only. This property was lost when inhibition was blocked by bicuculline thus indicating that it is mediated by $GABA_A$ receptors (**Yokoi et al., 1995**). Thus contrast enhancement in the bulb is proposed to be a competitive process between neurons processing similar information and helps in improving the molecular contrast between related compounds (**Cleland and Linster, 2005**).

Such contrast enhancement models are based on neurons sharing similar receptive fields and lying nearby to each other (topographically related), however it is unlikely that a fine chemotopic organization exists in the olfactory bulb. Studies done in zebrafish have shown that natural odors such as amino acids, bile acids and nucleotides activate different regions in the olfactory bulb and similar amino acids activate overlapping regions indicating presence of a coarse chemotopy (**Friedrich and Korsching, 1997, 1998**). Another study using optical imaging of intrinsic signals studied the activation of glomeruli in response to a series of aliphatic molecules which had the same functional group but different chain lengths. They found a clear relationship between glomerular region activated and its preferred chain length and there was a successive shift in the

glomerular region activated with increasing carbon chain length **(Meister and Bonhoeffer, 2001)**. However, another study using a marker for vesicle fusion reported results that were in disagreement with the above studies as they did not find any successive activation of glomeruli to a homologous chemical series **(Bozza et al., 2004)**. Since the odor is a multidimensional chemical stimulus there is difficulty in addressing this issue using a series of odorant stimuli that can be systematically varied along different dimensions.

The network architecture of the bulb can play a role in shaping the spatiotemporal patterns of activity. Insights into the relationship between dynamics and structure of complex networks can be gathered from the studies of Central pattern generators (CPGs). These are simple microcircuits which show rhythmic patterns of activity and their connectivity has been characterized in great detail by virtue of the fact they are comprised of a small population of neurons.

1.5 Structure Dynamics Relationship in Central Pattern Generators (CPGs)

CPGs are a group of neurons that generate rhythmic movement by activating motor neurons (which synapse onto the muscles) in a specific sequence. These include swimming, walking, heartbeat, chewing etc. **(Arbas and Calabrese, 1987; Marder and Calabrese, 1996; Miller and Selverston, 1982; Rabinovich et al., 2006; Satterlie, 1985**). The rhythmic movements occur due to the interplay of intrinsic properties of the constituent neurons and the circuit connectivity. In all of the pattern generators, the central feature is that neurons are synaptically coupled to each other through reciprocal inhibition. In certain CPGs, rhythms are shaped by the intrinsic pacemaker activity of the neurons whereas in others it arises as an emergent property of the inhibitory connectivity among the component neurons **(Marder and Bucher, 2001)**.

The pyloric rhythm of the crustaceans consist of alternating bursts of motor neurons generated by the stomatogastric ganglion (STG). The anterior burster neuron (AB) is an endogenous oscillator and is the main determinant of the pyloric rhythm. The AB neuron is electrically coupled to the pyloric dilator (PD) neurons and they together reciprocally inhibit other neurons in the network. This results in alternating bursting activity of different neurons in a specific temporal order, which is critical for the generation of the rhythm (Figure 1.3) **(Marder and Bucher, 2007; Miller and Selverston, 1982)**.

The gastric mill rhythm of crustaceans unlike the pyloric rhythm is an emergent property of the network and does not have any endogenous bursting neuron that determines the rhythm of the pattern. Gastric mill rhythm controls the movements of two lateral teeth and one medial teeth aiding in the grinding and chewing of the food (Figure 1.4) **(Heinzel, 1988; Marder and Calabrese, 1996; Mulloney and Selverston, 1974; Selverston and Mulloney, 1974).**

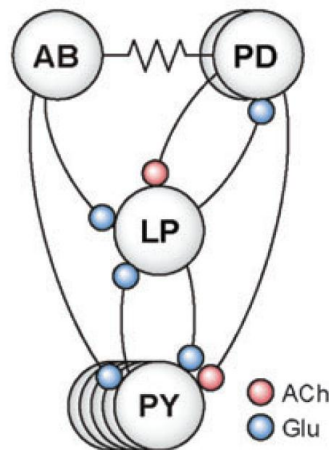**Figure 1.3 Connectivity Diagram of the circuit generating the pyloric rhythm**

AB is anterior burster neuron, PD is pyloric dilator neuron, LP is lateral pyloric neuron, PY is pyloric neurons. Reproduced from (Marder and Bucher, 2007) with permission.
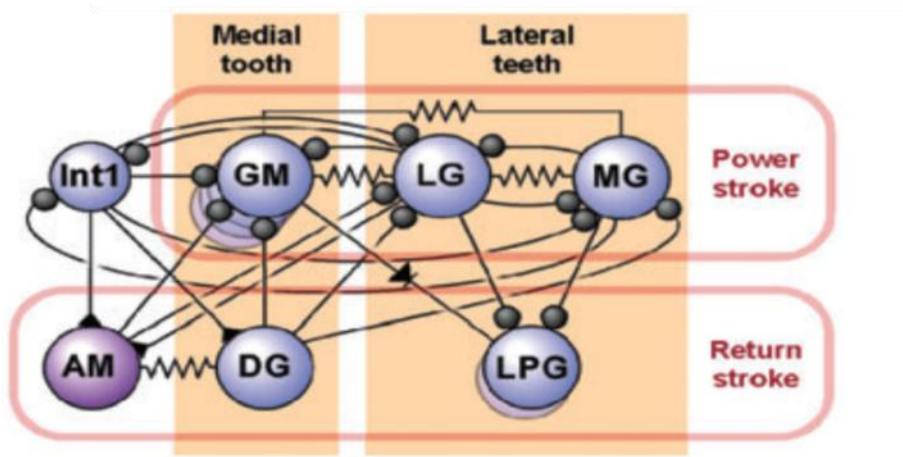
Figure 1.4 Connectivity Diagram of the circuit generating the gastric mill rhythm in crustaceans

Reproduced from (Marder and Bucher, 2007) with permission.

Studies of pattern generators have thus helped in understanding how reciprocal inhibitory networks give rise to sequential patterns of activity and has contributed to understanding similar phenomenon observed in various other brain regions.

1.6 Inhibitory Network Dynamics

A computational study has shown that graph coloring is a useful technique to study inhibitory network dynamics (**Assisi et al., 2011**). There are many types of graph coloring but the most commonly used one is vertex coloring. It involves assigning different colors to nodes which are connected to each other and the minimum possible number of colors required to color a graph is known as its chromatic number. The authors of the study used graph coloring to investigate structure dynamics relationship in the locust antennal lobe (**Assisi et al., 2011**). The antennal lobe consists of populations of inhibitory neurons known as LNs (local neurons) and excitatory populations known as PNs (principal/projection neurons). The LN population is connected to each other through reciprocal inhibition forming a sub-network and also sends inhibition to the PN population. The PN population sends excitatory connections to the LNs. Odors evoke spatiotemporal patterns of activity in the PN population. Computational studies of insect antennal lobe have shown that LN inhibitory network entrains different populations of PNs leading to their synchronization and temporal patterning (**Bazhenov et al., 2001**).Graph coloring helped in understanding how LN sub-network can give rise to this patterning. Groups of neurons that do not have any inhibitory connections among each other are assigned the same color whereas neurons with which they form reciprocal inhibitory connections are given a different color. Thus neurons associated with the same color fire synchronously whereas neurons associated with different colors fire at different times generating an ordered sequential activity. This relationship of coloring with the dynamics is easy to observe in regular networks or specially constructed networks. However, coloring random networks is a hard problem. Random networks can have multiple possible colorings and obtaining all possible colorings in a reasonable period of time is an intractable problem. It is also not guaranteed that a minimal coloring will always be achieved. To overcome limitations of graph coloring we turned our attention towards connectome studies which use graph theoretic measures to study brain structure dynamics relationship (**Bullmore and Sporns, 2009**).

1.7 Connectome Studies

Large scale synchronized activity has been observed in various brain regions and it is known to play a major role in information processing **(Singer, 1999)**. These coherent patterns of activity arise from the underlying neuronal structure. Connectomic studies aim to map the anatomical connections of the brain in order to understand how the network structure of the brain shapes its emergent properties. The anatomical connections are largely determined using tractography or diffusion tensor imaging (DTI). The anatomical connections, so found, are studied using graph-theorectic techniques. One of the widely used techniques are community clustering algorithms which help in characterizing organizational features of the connectome. These algorithms have helped in finding communities of neurons coupled through excitation, which cluster together with most edges lying within the module and minimal edges lying across the modules **(Sporns, 2013)**. These studies have revealed that a large number of motifs and modules exits within the cortical regions of the brain **(van den Heuvel and Sporns, 2013)**. The presence of modules indicates that there is segregation of information in the brain. The modules represent neurons which share common input and output connections and give rise to coherent patterns of activity **(Sporns, 2013)**. Another class of networks that are studied are known as functional networks. Connectivity in functional networks (functional connectivity) is determined by studying statistical dependencies among neuronal elements, correlations derived from time series data such as EEG (electroencephalography), magnetoencelphalography (MEG) and fMRI (functional magnetic resonance imaging) studies. Studies have found that a relationship exists between the anatomical connectivity and the functional connectivity. Functional connectivity is shaped by the underlying anatomical connections **(van den Heuvel and Sporns, 2013)**. Theoretical work has demonstrated how synchronization occurs in networks of complex topologies **(Arenas et al., 2008)**. These studies have helped in understanding the structure dynamics relationship observed between anatomical and functional connectivity.

The above studies have mainly looked into synchronization in networks which are coupled through excitation, however we study networks of inhibitory neurons. For inhibitory networks, communities are defined as groups of neurons which are maximally **disconnected** from each other and send most of the connections across the community and this is the modularity for inhibitory networks. Due to the limitations of graph coloring on random networks, we applied community detection algorithms for finding such groups of neurons in inhibitory networks.

1.8 Thesis Outline

It has been hypothesized that different odors activate different subnetworks in the olfactory bulb. We have tried to understand how the structure of the bulb circuitry through lateral inhibition gives rise to the dynamics (representations). Given that brain regions have modularity in their structure, using community detection algorithms we tried to establish a relationship between the modularity of inhibitory networks and the dynamics that are governed by it. Modularity of inhibitory networks is defined as the group of neurons that are maximally disconnected with each other in the group but their maximum connections lie in with neurons belonging to other group. Given that graph coloring is a complex problem and obtaining all possible colorings for random networks is computationally hard we have explored our methodology for random networks:

Chapter 2: In this chapter we describe the model of the mitral cells in detail and show how intrinsic properties determine the temporal sequences in a small random network of mitral cells.

Chapter 3: In this chapter using larger random networks we use a particular community clustering algorithm - Newman modularity algorithm and apply it to detect correlations between the structure and the dynamics of random networks.

Chapter 4: In this chapter we show the results of how introduction of asymmetry in the network topology leads to reliability of representations across noise perturbations.

Chapter 2: Spatiotemporal Patterning in the bulb

2.1 Introduction

It has been proposed that odor representation is converted from a combinatorial representation by ORNs to a spatiotemporal code in the OB/AL **(Laurent, 2002)**. Recordings done in the locust antennal lobe show that odor stimulation results in odor specific activation of PNs. The activated PNs do not fire continuously but fire at certain epochs of the entire duration of ensemble response. The slow temporal activity evolves along a fast oscillatory activity as observed in the local field potential. At each cycle of the oscillation the subset of synchronously firing PNs change. Thus, odor information is represented by spatial (PNs that are activated and participate in the ensemble response) and temporal activity (the order in which they fire) **(Laurent, 2002; Laurent et al., 1996b; MacLeod and Laurent, 1996; Wehr and Laurent, 1996)**. The synchronization of PNs is dependent on the inhibition mediated by the local neurons in the antennal lobe as was observed in the locust and honeybees **(MacLeod and Laurent, 1996; Stopfer et al., 1997).** Odor evoked oscillatory synchronization and its importance in odor encoding was shown in honeybees. Honeybees were trained to discriminate odors using a proboscis extension conditioning paradigm. Using this paradigm honeybees were able to discriminate between structurally similar odors (1-hexanol and 1-octanol) and a dissimilar odor which is geraniol (a terpene). When picrotoxin, an ionotropic GABA antagonist was injected into the antennal lobe this led to loss of oscillatory synchronization as was evident with no power at the stimulus evoked frequency in the power spectrum. The bees failed to discriminate between 1-hexanol and 1-octanol. However, they were able to discriminate between geraniol and hexanol. Thus loss of synchronization led to impairment in fine odor discrimination **(Stopfer et al., 1997)**. In an experiment done in rodents it was found that when rodents take longer time to make a decision for odor discrimination, higher inhibition leads to better performance in such a task **(Abraham et al., 2010; Abraham et al., 2004)**.

In this chapter we have constructed realistic biophysical models using in house developed neuronal C++ library in-silico to understand how intrinsic properties and lateral inhibition play a role in generating spatiotemporal patterning in the olfactory bulb.

The choice of using multicompartment models or reduced models for simulations depends upon the goal of the study. Multicompartment models are generally used for studying the properties of single neurons such as the role of different currents or dynamics of synaptic transmission. Reduced models or single compartment models are useful if one is interested in studying how the activity

of group of neurons give rise to properties such as synchronization. Single compartment models ignore detailed biophysical properties and take into account only those that are needed for spike timing (**Marder, 1998**). Bhalla and Bower described a 286 compartment model of the mitral cell obtained by fitting parameters based on the electrophysiological recordings and anatomical details of the cells (**Bhalla and Bower, 1993**). Since our study involves network behavior, we have used single compartment model of mitral cells.

2.2 Methods

In this study mitral cells were modeled as single compartment using voltage dependent currents that were based on Hodgkin Huxley kinetics: The current equation for the mitral cell model is as follows:

$$C_m \frac{dV}{dt} = -I_L - I_{Na} - I_{NaP} - I_{Kfast} - I_{Ka} - I_{Ks} - I_{syn} + current - noise$$

(1)

Equation 1 describes the dynamics of a mitral cell network comprising of N neurons.

The ionic currents governing the intrinsic dynamics are governed by the following equation:

$$I = g_{max} m^M h^H (V - E)$$

(2)

E denotes the reversal potential and g_{max} denotes the maximal conductance of the channel. **m** and **h** are the time and voltage dependent gating variables (M and H represent the number of activating and inactivating gates respectively).

The gating variables are given by the following ODE's:

$$dm/dt = (m_\infty - m)\tau_m$$

$$dh/dt = (h_\infty - h)\tau_h$$

$$m_\infty = \alpha_m(V)/(\alpha_m(V) + \beta_m(V))$$

$$\tau_m = 1/(\alpha_m(V) + \beta_m(V))$$

$$h_\infty = \alpha_h(V)/(\alpha_h(V) + \beta_h(V))$$

$$\tau_h = 1/(\alpha_h(V) + \beta_h(V))$$

Sodium Current:

$I_{Na} = g_{Na}m^3h(\text{V-}E_{Na})$

$\alpha_m = \dfrac{0.32(V + 50)}{\left\{1 - \exp\left[-\dfrac{V + 50}{4}\right]\right\}}$, $\beta_m = 0.28(V + 23)/\{\exp[(V + 23)/5] - 1\}$

$\alpha_h = 0.128/\exp[(V + 46)/18]$, $\beta_h = 4/\{1 + \exp[-(V + 23)/5]\}$

$g_{Na} = 50 \ mS/cm^2$, $E_{Na} = 45 \ mV$

Persistent Sodium current:

$I_{Nap} = g_{NaP}m(\text{V-}E_{NaP})$

$m(V) = 1/\{\exp[-(V + 51)/5] + 1\}$

$g_{NaP} = 0.1 \ mS/cm^2$, $E_{NaP} = 55 \ mV$

KA current:

$I_{Ka} = g_{Ka}mh(\text{V-}E_{Ka})$

$\tau_m(V) = 25 \exp[(V + 45)/13.3]/\{\exp[(V + 45)/10] + 1\}$

$\tau_h(V) = 55.5 \exp[0.99(V + 70)/5.1]/\{\exp[(V + 70)/5] + 1\}$

$m_\infty = 1/\{\exp[-(V - 70)/14] + 1\}$

$h_\infty = 1/\{\exp[(V + 47.4)/6] + 1\}$

$g_{Ka} = 10 \ mS/cm^2$, $E_{NaP} = -70.0 \ mV$

KS current:

$I_{Ks} = g_{Ks}mh(V - E_{Ks})$

$$\tau_m(V) = 10$$

$$\tau_h(V) = 400 + 110/\{\exp[-(V + 71.6)/6.85] + 1\}$$

$$m_\infty = 1/\{\exp[-(V + 34)/6.5] + 1\}$$

$$h_\infty = 1/\{\exp[(V + 65)/6.6] + 1\}$$

$$g_{Ks} = 31 \, mS/cm^2 \, , \, E_{Ks} = -70.0 \, mV$$

Kfast current:

$$I_{Kfast} = g_{Kfast}m^2h(V - E_{Kfast})$$

I_{Kfast} kinetics were modeled using a table which was adapted from Bhalla and Bower 1993. (Details provided in Appendix)

$$g_{Kfast} = 50 \, mS/cm^2 \, , \, E_{Ks} = -70.0 \, mV$$

Synapse:

Synaptic conductance is modeled as a difference of two exponential functions of time t

$$g(t) = \frac{g_{syn} \, \tau_r \, \tau_d}{\tau_r \, \tau_d} \, [\exp(-t/\, \tau_d) - \exp(-t/\tau_r)]$$

where τ_r and τ_d are the rise time and fall time of the synapse respectively. g_{syn} is a factor dependent on rise and fall time such that the maximal value of g(t) is 1 with respect to time. Its value used in the model is 5.2381. The synaptic current is given by:

$$I_{syn} = g_{synmax}g(t)(V_{post} - E_{GABA})$$

where g_{synmax} is the maximal synaptic conductance. The inhibitory synaptic current is activated by presynaptic spikes in the mitral cell. The reversal potential for GABAergic synapse is -70.0 mV. The rise time is 0.2ms and the decay time is 20ms with a latency of 0.75ms.

Simulation procedure:

All single cell and network simulations were carried out using a fourth order Runge Kutta integration method. Time step used for simulation was 27µs. The input onset was set at 1000ms so as that the cells settle down to resting state. The input was provided for 6000ms and started to decay at 7000ms. Simulations were performed using an in house developed open source C++ library called '**in-silico'**. The in-silico library utilizes the boost library (odeint) for integrating the system of coupled differential equations. MATLAB was used to visualize and analyze data.

2.3 Results

2.3.1   Mitral cells show mixed mode oscillations

Using a minimal set of parameter values the model recaptures some of the essential physiological properties of mitral cells. It includes the regular spiking current (I_{Na}), a delayed rectifier (I_{Kfast}), a leak current (I_{Leak}), slow potassium(I_{Ks}) and persistent sodium (I_{Nap}) current. An additional A-type potassium current has also been included (Figure 2.1). The model is based on a previously published study by Bathellier et.al. (**Bathellier et al., 2006**). The activation and inactivation curves of sodium (I_{NA}) and delayed rectifier potassium current (I_{Kfast}) have been shifted by -8mv to lower the spike threshold in accordance with the experimental results (**Desmaisons et al., 1999**). The I_{Ka} current is responsible for the delay in onset of spikes (**Balu et al., 2004).**
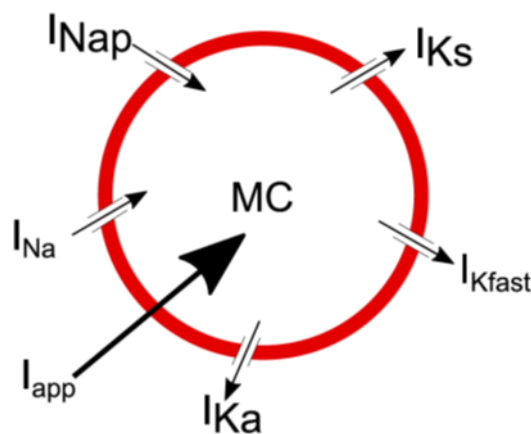

Figure 2.1 Schematic of the currents present in the point model of mitral cell

Currents in the model are sodium (I_{Na}), delayed rectifier (I_{Kfast}), leak current (I_{Leak}), slow potassium (I_{Ks}), persistent sodium (I_{Nap}) and I_{Ka}. I_{app} is the applied current.

Olfactory sensory neurons excite the mitral cells through the neurotransmitter glutamate **(Berkowicz et al., 1994)**. The input provided to the mitral cells was a depolarizing current which had an onset time (1000ms), a particular peak amplitude (0.6μA) and a fall time (7000ms). Upon depolarizing the mitral cells, they showed repetitive firing of clusters of action potentials interspersed with epochs of subthreshold oscillations (STOs) which match with the experimental recordings **(Chen and Shepherd, 1997; Desmaisons et al., 1999)**. This rhythmic activity is known as mixed mode oscillations (Figure 2.2). This alternation of burst of spikes followed by subthreshold oscillations results because of the slow timescale of the potassium current (I_{Ks}). Slow potassium current is a depolarization activated hyperpolarizing current. Due to the slow timescale of the inactivation variable the I_{Ks} builds up slowly at each successive spike and after certain number of spikes it causes cessation of spikes in the cell and the neuron goes into STO mode (Figure 2.3). After spike cessation, there is a gradual decline in the inactivation variable of the slow potassium current. Since the neuron receives an input the membrane potential is depolarized by the applied current, which is further amplified by the persistent sodium current. This small depolarization activates the slow potassium current which again leads to hyperpolarization of the membrane voltage. This back and forth depolarization and hyperpolarization is responsible for the generation of STOs. Decay in slow potassium current leads back to the appearance of spike clusters and the whole cycle repeats. It has been shown that subthreshold oscillations are generated by interaction between a resonant current and an amplifying current **(Hutcheon and Yarom, 2000)** and in our model the resonant current is I_{Ks} and the amplifying current is I_{Nap}. Mixed mode oscillations are also seen in the stellate cells, found in the entorhinal cortex, where they are generated by the interaction of I_H and I_{Nap} current **(Dickson et al., 2000)**.
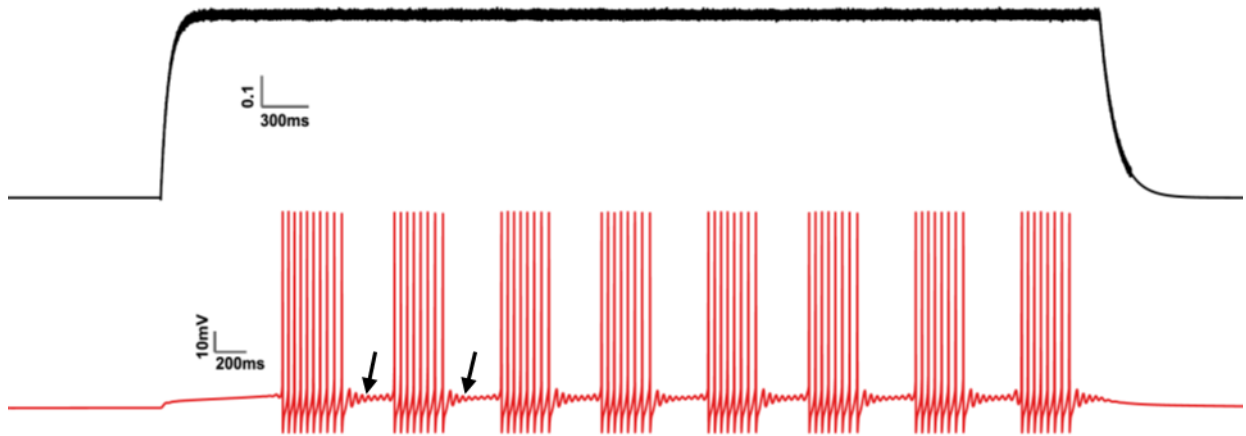
Figure 2.2 Mitral cells display spiking as well as subthreshold oscillations

Top panel shows the depolarizing input current given. It has an onset time and an offset time.

Bottom panel shows the firing of mitral cell in response to a current of amplitude 0.6μA. Mitral cells respond with clustering of action potentials interspersed with subthreshold oscillations. Arrows indicate the subthreshold oscillations.
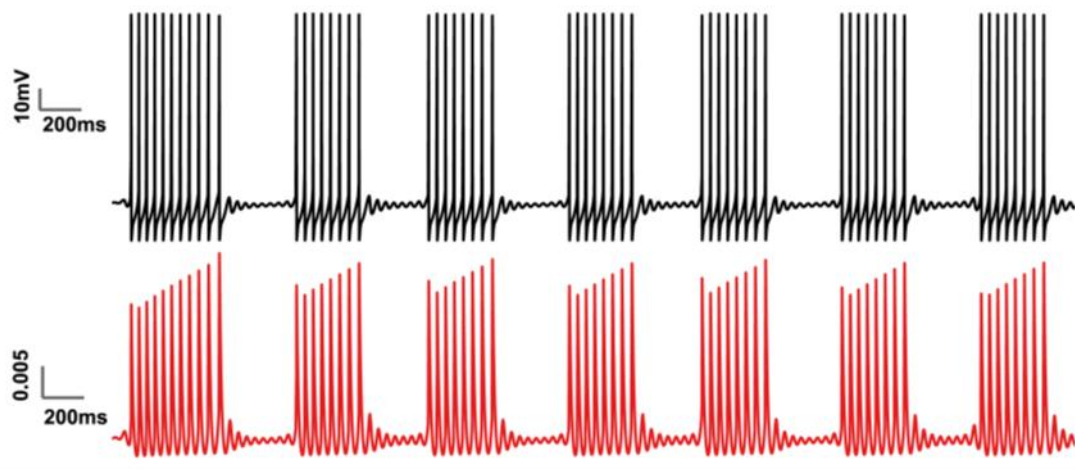
Figure 2.3 Mitral cell activity and the role of I_{Ks} in generating mixed mode oscillation

Top panel mitral cell activity.

Bottom panel shows open fraction channel of I_{Ks} current. After certain successive action potentials the I_{Ks} current builds up and causes cessation in activity of the mitral cell which is followed by subthreshold activity.

2.3.2   Mitral cells inhibit each other and display antagonistic interactions

Granule cells mediate recurrent as well as lateral inhibition onto mitral cells belonging to other glomeruli. . There are no granule to granule cell connections thus far found **(Neville and Haberly, 2004)**. Thus mitral cells inhibit each other through granule cells. We have not explicitly modeled the granule cells in our simulations. We have assumed that mitral cells are coupled to each other via lateral inhibition. Lateral inhibition between mitral cells is the sum of small inhibitory postsynaptic currents (IPSCs) mediated by GABAergic interneurons through dendrodendritic coupling. Our parameter values for lateral inhibition are not based on real experimental data hence we derive conclusions that are not dependent on the particular parameter value chosen but are based on general observations.

We started with the simplest motif of two mitral cells (M1 and M2) inhibiting each other through lateral inhibition. On driving the two mitral cells with a depolarizing current they showed alternation in their activity. How does this alternation/switching in the activity arise? When M1 neurons fires because of inhibition M2 remains in a quiescent state. When M1 is spiking the slow potassium current of M1 builds up and after a certain number of spikes it switches of the M1 neuron and the M2 neuron escapes from inhibition and starts spiking (Figure 2.4). In our parameter regime the two neurons continue to switch for the duration of the stimulus and neither of them completely suppress each other.

Antagonistic interactions between neurons can also occur through spike frequency adaptation. Spike frequency adaptation is a prominent phenomenon seen in the dynamics of neurons and is exhibited by different types of spiking interneurons. Spike frequency adaptation is mediated by a number of ionic currents such as the slow recovery from inactivation of fast sodium current, M-type currents and calcium dependent potassium currents (AHP) **(Brown and Adams, 1980; Fleidervish et al., 1996; Madison and Nicoll, 1984)(see (Benda and Herz, 2003)review on detailed mechanisms of spike frequency adaptation)**. In a model of locust antennal lobe switching in the dynamics of LNs occurs through a hyperpolarizing calcium dependent potassium current **(Assisi et al., 2011)**.
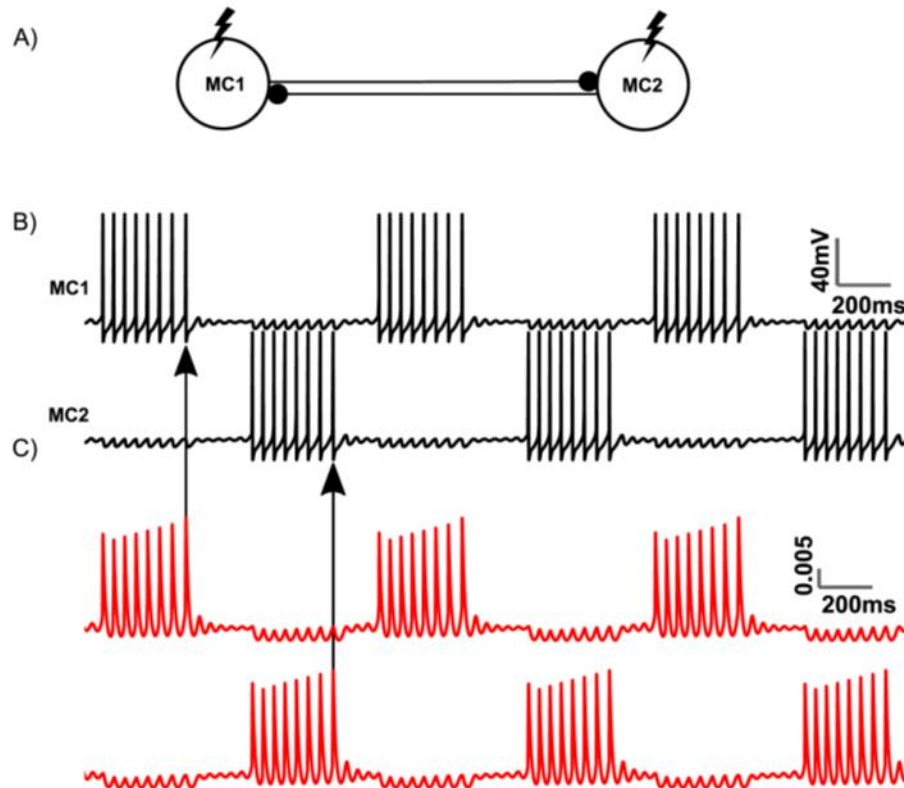
Figure 2.4 Switching Dynamics in Mitral Cells

A) Schematic of two mitral cells reciprocally inhibiting each other.

B) Reciprocally connected mitral cells generate alternating bursts of activity.

C) The open fraction of slow potassium current. It is a depolarization activated hyperpolarization current. It builds up with each successive spike of the mitral cell and switches off the neuron (indicated by the arrows) after some time which leads to alternation in spiking activity.

2.3.3   Temporal sequences in a mitral cell network

Odors evoke spatiotemporal patterns of activity in the mitral cells. To examine the factors that give rise to temporal ordering we used a random motif of six mitral cells which are coupled to each other via lateral inhibition (Figure 2.5A). Upon injecting a depolarizing current to all the neurons we observe a temporal sequence of neuronal activity. This temporal patterning results because of the interplay of lateral inhibition and the slow potassium current dynamics. The neurons organize themselves into three groups, as shown by the color coding scheme (Figure 2.5). Neurons having the same color fire synchronously and alternate with neurons associated with other colors, which fire at different times. This shows that neurons that are not inhibiting each other do not compete with each other and fire together. The activity of neurons largely follows the topology but due to the difference in synaptic weights we get three different groups. The temporal ordering in the motif is determined by the relative activation of the slow potassium current. The neuron that fires immediately is determined by the one whose inactivation variable has the lowest value (Figure 2.5B). Our motif was able to generate the spatiotemporal patterns as evidenced by epochs of excitation and inhibition of neurons observed in the recordings of the mitral cells upon odor activation **(Friedrich and Laurent, 2001)**. In the insect antennal lobe the ordering is determined by the calcium concentration. The neuron with the lowest calcium concentration is the one that is most likely to fire **(Assisi et al., 2011).**

Temporal ordering can also be determined by other factors such as the asymmetries in the input pattern, asymmetries in the intrinsic properties of neurons or network topology.
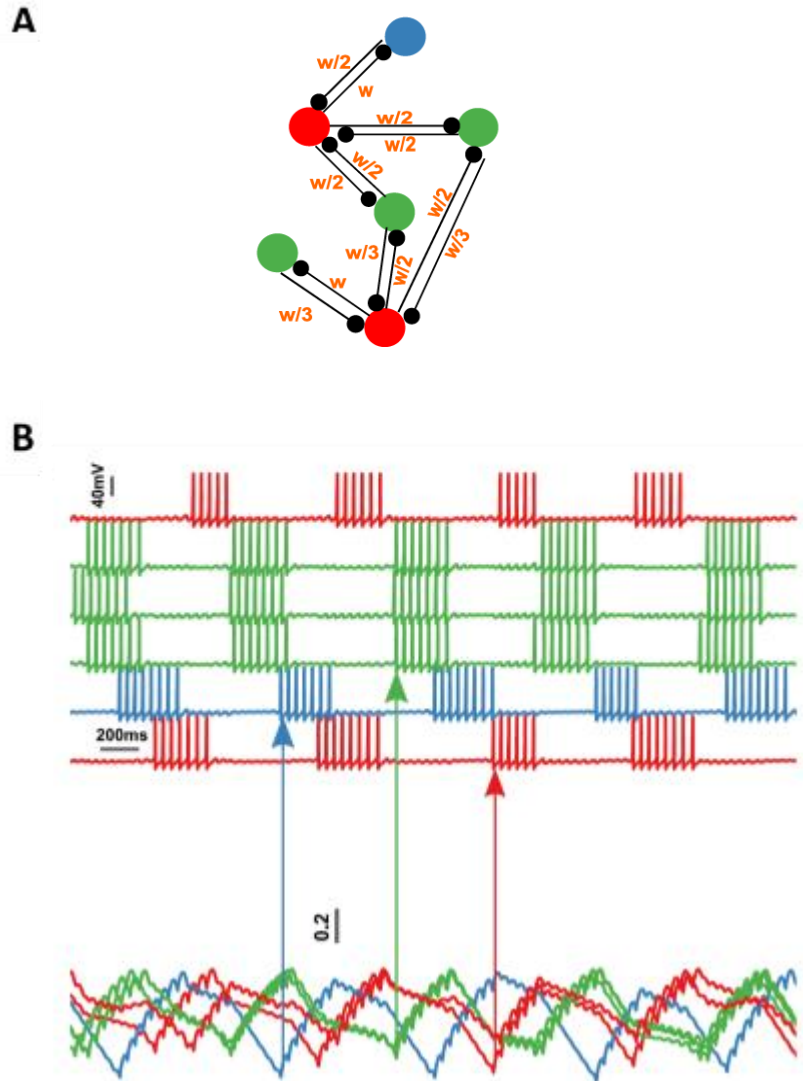
Figure 2.5 Temporal ordering in a network of mitral cells

A) Schematic of the connectivity of a random network of 6 mitral cells. w indicates the weight of synapse (w=4.2 mS/cm^2).

B) Mitral cell network is capable of generating a sequence which is dictated by the inactivation variable of the slow potassium current. The **top traces** (top 6) show the activity of the mitral cells which follows a particular sequence. The neuron that spikes immediately after a particular neuron is the one whose inactivation variable has the lowest value (**bottom traces**) among all neurons.

2.4 Summary

We have used realistic biophysical models of the mitral cells which capture the physiology of the mitral cells (mixed mode oscillation). Based on these results we proceeded to study and characterize the dynamics in larger networks of mitral cells.

Chapter 3: Clustering in Inhibitory Networks

3.1 Introduction

Inhibition plays an important role in spatiotemporal patterning in a number of neuronal networks (for example in case of central pattern generators involved in chewing, locomotion, swimming). In the locust antennal lobe Assisi et. al. derived a simple relationship between the structure of the inhibitory network and the collective dynamics of neurons that form the network (**Assisi et al., 2011**). Antagonistic interactions between inhibitory interneurons imply that neurons that were directly connected to each other did not spike at the same time. This could be related to a structural property of the network, namely the coloring. Graph coloring is a partitioning of the network that assigns different colors to nodes that are directly connected. Nodes of different colors, due to inhibition, fire at different times whereas those that do not connect can potentially spike synchronously. The relationship between the coloring and the dynamics of the network is easy to observe in case of small or regular networks. However, coloring networks with a complex topology is a difficult problem since there are many possible solutions (colorings) and determining all these colorings in a reasonable period of time is an intractable problem. Despite these technical hurdles, coloring provides a useful heuristic to examine the structure of inhibitory networks.

Consider a densely connected network of neurons that interact via excitation. These would tend to fire in a correlated manner. Similarly, in resting state networks correlated dynamics are often used to identify functionally connected components of the network (**Deco et al., 2011; Sporns, 2013**). Given that dynamic correlations are often a signature of physical connections between components, a number of algorithms that characterize the structure of brain networks look for modules– densely connected sub-graphs that extend sparse connections to other nodes of the graph. A coloring can be thought of as a module with just the opposite property – Nodes that do not connect to each other tend to form synchronously spiking groups. This peculiar property meant that we could still employ the same modularity detection tools, but on networks that were 'flipped' versions of the inhibitory networks –nodes that were not connected in the original network would be connected in these flipped networks. We posit that the dynamics of modules detected by clustering algorithms - densely connected sub-graphs of the flipped network – would be correlated since they do not inhibit each other. This technique certainly does not detect the colorings of the original network, but it can potentially identify clusters of neurons that fire in a correlated manner.

In the following section we describe various algorithms that are commonly used for clustering and studying the properties of networks.

3.2 Clustering methods

A graph is an ordered pair G = (V, E) where V is a set consisting of elements known as *vertices* or *nodes* and E is a set consisting of elements known as *edges/links* between these vertices. Since many widely studied natural systems can be represented as networks, graph theoretic techniques are widely used to study problems in different areas like biology, engineering, physics and sociology.

Some of the widely used methods are concerned with clustering/partitioning of networks. Partitioning is done to study the organizational features of the network which are not obvious in the raw network topology. This can help in getting valuable information, for example presence of distinct communities means that different functionalities are present in the network. Detection of groups in networks has been done using two principal methods known as graph partitioning algorithms and community detection algorithms. The aim of both these methods is to find divisions of the network such that they reveal densely connected groups with sparse connections across groups. However there exist some differences between the two methods. Graph partitioning algorithms always gives a partition of the network even if no good division is permissible. For these algorithms the experimenter should *a priori* provide the number of groups and group sizes into which the network should be split. These algorithms have been typically useful for computer science problems, for example in case of parallel computing where the computations are to be split among different processors in such a manner that there is minimal interprocessor communication. This increases computational efficiency and performance. The investigator knows beforehand the number of processors and the number of jobs to be assigned to each processor, thus the number of groups and the group sizes is *a priori* known. These algorithms are not useful when the experimenter does not know into how many different groups to split the network and the size of the groups. On the other hand, for community clustering algorithms the investigator is not required to *a priori* specify the number of groups and their sizes. These algorithms work on the premise that "natural groupings" exist in the network and the objective is to find them. If there is no good partition possible these algorithms do not force a division of the network. These algorithms find communities based on the idea that the communities so found have fewer than expected number

of edges across them. For this purpose the community structure of the network is compared with a null model. A null model is a randomization of the original network wherein the degrees of the nodes are preserved. If the number of edges within the communities is significantly more (alternatively number of edges across communities is significantly less) than expected chance, then it is said that the communities found are meaningful in nature (it is assumed that the null model will not have a community structure). A quantity known as modularity has been defined for these algorithms. This quantity reveals the goodness of the partition and hence the partition corresponding to the maximum value represents the best possible clustering of the network. Therefore most of these algorithms try to partition the network in such a manner that this quantity is maximized. Finding the true modularity is time consuming and a difficult problem. Therefore most of the algorithms try to find approximate solutions to the maximum modularity value which is acceptable in most cases. Hence these algorithms are also known as "heuristic algorithms" **(Fortunato, 2010; Newman, 2006, 2010)**.

Below we review some of the algorithms with their methodology of finding clusters and some of their drawbacks and why we choose a particular algorithm for our work.

3.2.1 Kernighan-Lin Algorithm

Kernighan-Lin is a graph partitioning algorithm developed by Brian Kernighan and Shen Lin in 1970. The algorithm finds clusters by optimizing a benefit function (Q) which is defined as the difference between the number of edges within the clusters and the number of edges across the clusters. At the start the algorithm requires that the user specifies the size of the groups and for initial configuration the vertices are randomly assigned to the two groups. There are two stages in this algorithm. In the first stage, for each possible pair of vertices selected from the two groups, the change in the benefit function is calculated if those two vertices were swapped. Then the pair for which the change is the highest is selected and swapped. This way the algorithm does not change the size of the groups and maintains the partitioning originally specified. After this, the procedure is again repeated with the condition that the pair of vertices once swapped will not be used again. In the second stage, after all the swaps have been completed the algorithm goes back through all the swapping stages and finds the point at which Q was highest. This is the final partition of the network.

This algorithm suffers from some drawbacks. It is unsuitable for situations where the investigator does not have a clue about the sizes of the groups. The experimenter is forced to choose particular group size, which can lead to unwanted results. In such cases the algorithm can be run against all possible partitions of the network but not only would that be time consuming, the best values of Q are achieved for partition into highly asymmetric group sizes. The other drawback is that this algorithm only results in division of the network into two groups. Further division of the network could be achieved by repeatedly bisecting the groups thus found, but there is no assurance that the procedure followed this way will result in the best division of the entire network. Also the user does not know when to stop this process of repeated bisections **(Kernighan and Lin, 1970; Newman, 2010; Newman, 2004).**

3.2.2 Agglomerative/Hierarchical clustering

Hierarchical clustering is an agglomerative technique which involves joining of nodes to each other in a hierarchical manner based on a similarity measure until all the nodes are joined forming one single large cluster. This leads to a tree like representation known as dendrogram from which clustering can be inferred. This approach has been described as bottom up approach of clustering. This algorithm stands in contrast to other graph partitioning algorithms which are divisive techniques as they take a network and fragment it into different parts. The connections made between the nodes in this method has no relation with connections in the original graph. The original graph connections are used only for calculating the similarity measure. There are number of different similarity measures available to the experimenter to select for his task. The choice is dependent on the requirements of the problem. Some of the most commonly used measures are Euclidean distance, Hamming distance, Mahalanobis distance, Minkowski distance, Square-euclidean distance etc. The algorithm first starts by calculating the similarity scores for all pairs of vertices in the network. It then joins the vertices with the highest similarities to form a group. Further, groups that are most similar are combined together forming larger clusters and this process is repeated until all vertices have been taken into account. Once the dendrogram is created, cutting the tree by choosing a particular point reveals the clusters (following the branches shows the clusters). This process of joining groups requires calculating similarity measure for the groups. Three different methodologies exist for calculating group similarity scores:

1. Single linkage clustering: In this method similarity of two groups is taken to be the highest similarity value of all the vertex pairs

2. Complete linkage clustering: In this method similarity of two groups is taken to be the least similarity value of all the vertex pairs

3. Average linkage clustering. In this method the similarity of two groups is the average similarity value of all vertex pairs. This method creates a balance and is not at the extreme ends like single linkage and complete clustering.

To summarize the algorithm for this clustering method is:

1. Choose a similarity/dissimilarity measure to be applied on all pairs of nodes
2. Compute the similarity/dissimilarity measure for all nodes pairs of the network.
3. Using the computed score choose the pair with the highest similarity measure and group them into a single cluster.
4. Calculate the new similarity measure for this composite group and other nodes using the methods mentioned above (single, complete and average linkage).
5. Keep repeating from step 3 onwards till a single group is achieved.

This method has the advantage that the experimenter is not required to input the size and number of groups in advance, however it does have some drawbacks. Hierarchical clustering, despite offering a number of different similarity metrics and linkage methods to choose from does not specify which metric and method is best suited for a particular problem. Also, the experimenter does not know into how many communities the network should be split for the best result. The other problem with hierarchical clustering is that it can result in single nodes which are not part of any group. This is because it generally clusters nodes which have strong similarity scores together leaving the assignment of single nodes (also called peripheral nodes) towards the end of the clustering process because of their low similarity values **(Fortunato, 2010; Newman, 2010).**

3.2.3 Girvan Newman Algorithm

The Girvan Newman algorithm is a community detection algorithm that finds "natural divisions" of the network. As seen in hierarchical clustering this algorithm also generates a dendrogram as

its output. It is however a divisive algorithm as it involves a top down approach by starting at the very top of the tree (known as the root) and going all the way down to the bottom (the nodes are known as leaves). This algorithm operates on the principle that if the information has to flow between nodes belonging to different communities it will occur through the shortest path and the paths will involve edges connecting those communities. The goal is to find the edges which have a heavy flow of traffic and remove them, as this will help in unveiling the communities present in the network. For this the algorithm utilizes a quantity known as edge betweenness. Edge betweenness for a particular edge is defined as the number of shortest paths between all pairs of vertices in the network that goes through the edge in question. Higher edge betweenness score indicates that large information flows through that particular edge.

The algorithm works by first calculating the edge betweenness score for all edges in the network. Then the edge with the highest score is removed first. After removal the scores for the remaining edges is recalculated since the shortest paths between nodes will change. Then a search is again made to find the edge with the highest score and it is removed. This process of recalculating and removing of edges continues until there are no more edges left. The result is a dendrogram in which the branching reveals the order of splitting of the network. Horizontal cut in the dendrogram represents the possible community divisions with varying sizes of the communities.

This cut can be applied anywhere in the dendrogram and the investigator has the option to split the network as per their wish. However, it suffers from the same problem as hierarchical clustering, as the investigator does not know the best division. To address this problem Girvan and Newman modified this algorithm to introduce a parameter called the modularity value Q. Q is defined as the difference between the number of edges found within communities and the expected value in the same network where node degrees are preserved but edges are placed randomly. The other disadvantage of this algorithm is that the runtime scales with network size thus making it slow in operation **(Girvan and Newman, 2002; Newman and Girvan, 2004; Newman, 2004).**

3.2.4 Newman Modularity Algorithm
This algorithm is a modularity (Q) optimization method and finds communities based on the same premise that the number of edges found in a community is higher than the expected value of a

similar network in which edges are placed randomly and the node degrees are preserved. Modularity is calculated as the fraction of edges and not the number.

Modularity (Q) of a network is defined as follows:

$$Q = \frac{1}{4m} \sum_{ij} (A_{ij} - \frac{k_i k_j}{2m}) s_i s_j$$

Where A is the adjacency matrix, $\frac{k_i k_j}{2m}$ is the expected probability of connection between nodes i and j. m is the total number of edges in the network and k is the degree of each node. s is an index vector denoting the division of the network into communities. s is constrained to take values ± 1. If it belongs to community 1 then the element $s_i = 1$ and $s_i = -1$ if it belongs to community 2.

Figure 3.1 shows a schematic flow of how the Newman modularity algorithm works in detecting communities. As seen in the schematic the first step involves bisection of the network. This bisection occurs only if the modularity value increases.

The modularity can be rewritten in the matrix form as

$$Q = \frac{1}{4m} s^T B s$$

Where the entries of each element of B are as follows:

$$B_{ij} = A_{ij} - \frac{k_i k_j}{2m}$$

B is called the modularity matrix. Since the goal is to maximize the modularity this can be achieved by selecting the best partition and therefore the s vector should be chosen accordingly. Since modularity can be expressed in terms of the product of eigenvectors and s vector, the algorithm calculates the leading eigenvector (eigenvector with the most positive eigenvalue) to maximize the product. Since s is constrained to take only +1 or -1, s is made as close to parallel to the leading eigenvector as possible. For this the element of s vector is assigned +1 if the corresponding element in the eigenvector is positive, otherwise it is assigned -1. Thus the elements which are +1 in s go in one group and the negative elements go to the other group and the partitioning is achieved. If the algorithm is able to find no positive eigenvalue then it gives the trivial solution;

which is putting all the vertices into one community, meaning it is best to leave the network undivided.

The next step as seen in the schematic is to find further divisions of the communities. This is accomplished by examining each community and bisecting them with the constraint that division into further communities should result in an overall positive change in modularity which is given by the following equation:

$$\Delta Q = \frac{1}{4m} \sum_{i,j \in g} \left[B_{ij} - \delta_{ij} \sum_{k \in g} B_{ik} \right] s_i s_j$$

$$= \frac{1}{4m} s^T B^{(g)} s$$

Where δ_{ij} is kronecker δ-function and $B^{(g)}$ is n_g x n_g matrix indexed by i,j vertices of group g and its entries are given by:

$$B_{ij}^{(g)} = B_{ij} - \delta_{ij} \sum_{k \in g} B_{ik}$$

For further division the algorithm again looks for the leading eigenvector which will give positive value to the quantity ΔQ. As can be seen in Figure 3.1 the best partition of the given network is its division into three communities. The algorithm stops further subdivisions only when no positive contribution to the quantity ΔQ is found (**Newman, 2006**).

To summarize, this algorithm works by first constructing a modularity matrix from the adjacency matrix and finding the leading eigenvalue and the corresponding eigenvector. The network is then divided into two groups based on the signs of the eigenvector. This same operation is performed for finding subdivisions of the communities. If at any point the change in modularity is zero the division of that community is halted. The algorithm ends when the entire network has been split into indivisible communities.

This algorithm does not require the investigator to input the size and number of groups to start with and finds the natural communities present in the network. This algorithm is quite fast and the only time consuming step is finding the leading eigenvector. Thus the running time of this

algorithm does not scale with increase in network size. Based on these characteristics we chose this algorithm for our work.
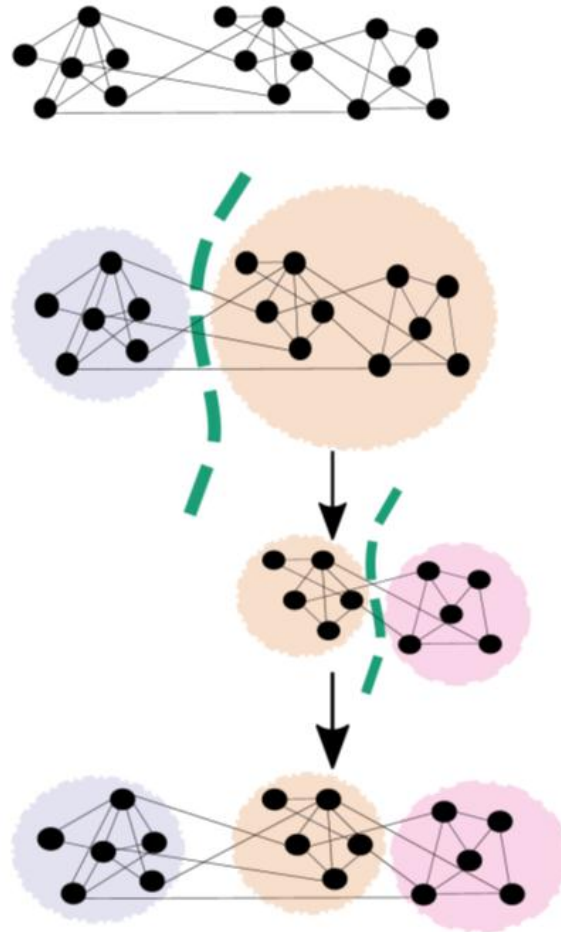
Figure 3.1 Schematic illustration of the Newman community detection Algorithm

 (Newman, 2006)

The diagram shows flow of the algorithm in detecting the underlying communities in the network. The algorithm works on the principle of repeated bisection of the network at each step to find communities. The top network shows the input network given to the algorithm. On the first iteration the algorithm divides the network into two communities on the condition that it leads to an increase in modularity. In the next iteration it examines each community separately found in the first step and tries to split it on the condition that it leads to an overall increase in modularity. The end result at the bottom shows the communities found by the algorithm.

3.3 Methods

Mitral Cell Model and synapse model:

These are described in chapter 2.

Network Structure:

We constructed random networks using the Watts and Strogatz model (**Watts and Strogatz, 1998**). This model starts with N nodes arranged on a circular ring and each node is connected to its k nearest neighbors. This network is also referred to as a regular network. In this regular network a particular node and the edge that connects to its nearest neighbor is chosen. With a particular probability β this edge is then rewired to a uniformly picked random node from the entire network or it is left unchanged. Moving in the clockwise direction the process is similarly repeated for all the other nodes. The first iteration is completed when the nearest neighbor edges of all the nodes are considered. In the next round edge that connects to the second nearest neighbor is selected and the similar operation of rewiring is applied. This process is then continued upon other nodes and after each round the next nearest neighbor edges are picked. The entire process of rewiring is completed when all the edges in the original network have been considered. Figure 3.2 illustrates the process of generating random networks using this model. The rewired network enters the random regime when β >=0.8. The random networks used for simulations in this chapter consisted of 50 neurons, K=6 and the probability β was 0.8.
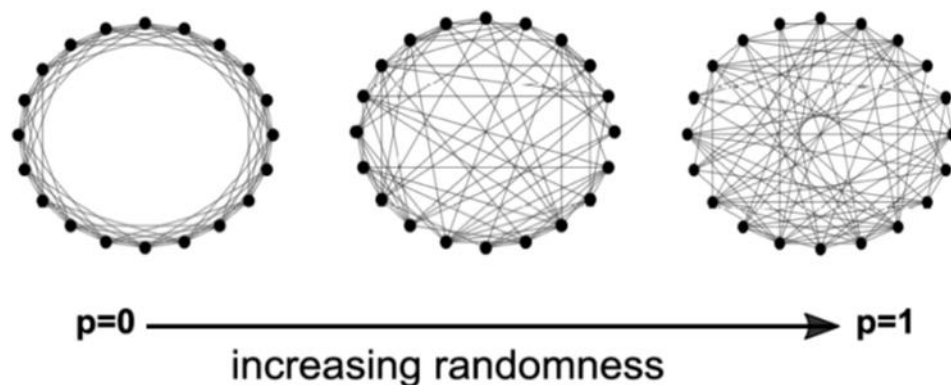

Figure 3.2 Watts and Strogatz model

A ring network of N nodes is constructed in which each node connects to k nearest neighbors (N=50, K=6 for our network. Three different realization of p have been shown here. When p>=0.8 the network becomes random.

Newman Clustering:

We have used MATLAB implementation of the Newman clustering algorithm from the Brain connectivity toolbox **(Rubinov and Sporns, 2010).**

Classical MultiDimensional Scaling (CMDS):

Classical Multidimensional scaling is a dimensionality reduction method which maps a higher dimensional data set to lower dimensions (up to three dimensions) by preserving the distances between points. CMDS uses eigenvalue decomposition for dimensionality reduction and requires the input as a distance measure which is usually the Euclidean distance. In our analysis we have used dissimilarity values as the distance measures for applying CMDS. We have used an R implementation of CMDS for the analysis.

Spike Synchrony:

Spike synchronization measures how synchronized the spike trains are. Values that are close to 1 imply that spikes are synchronous. A coincidence detection value is calculated for every spike in a spike train. Spikes $t_i^{(1)}$ and $t_j^{(2)}$ are coincident only if the difference in their spike times is below a threshold window $\tau_{ij}^{(1,2)}$ as given below

$$C_i^{(1)} = \begin{cases} 1 & if \ min_j \left(\left| t_i^{(1)} - t_j^{(2)} \right| \right) < \tau_{ij}^{(1,2)} \\ 0 & otherwise \end{cases} \text{ and analogously for } C_j^{(2)}$$

$$\tau_{ij}^{(1,2)} = \min\left\{ t_{i+1}^{(1)} - t_i^{(1)}, t_i^{(1)} - t_{i-1}^{(1)}, t_{j+1}^{(2)} - t_j^{(2)}, t_j^{(2)} - t_{j-1}^{(2)} \right\} / 2$$

$C_i^{(1)}$ is the coincidence value of ith spike in spike train 1.

$t_i^{(1)}$ is spike time of ith spike in spike train 1 for which coincidence value is being calculated.

$t_j^{(2)}$ is the spike time of corresponding spike (termed jth) in spike train 2 with which comparison is made

$t_{i+1}^{(1)}$ is the spike time of i+1 spike in spike train 1

$t_{i-1}^{(1)}$ is the spike time of i-1 spike in spike train 1

$t_{j+1}^{(2)}$ is the spike time of j+1 spike in spike train 2

$t_{j-1}^{(2)}$ is the spike time of j-1 spike in spike train 2

The spike synchronization for cases involving more than two spike trains is calculated by first performing bivariate coincidence detection for each pair of spike trains (n,m)

$$C_i^{(n,m)} = \begin{cases} 1 & if\ min_j\ \left(\left|t_i^{(n)} - t_j^{(m)}\right|\right) < \tau_{ij}^{(n,m)} \\ 0 & otherwise \end{cases}$$

This is followed by normalizing each coincidence values involving spike train n by averaging it over N-1 bivariate comparison:

$$C_i^{(n)} = \frac{1}{N-1} \sum_{m \neq n} C_i^{(n,m)}$$

N is the total number of spike trains being compared.

The coincidence detection values of both the spike trains are pooled together into a unified set of coincidence detectors.

Spike synchronization S is calculated as follows:

$$S_c = \frac{1}{M} \sum_{k=1}^{M} C(t_k)$$

M denoting the total number of pooled spikes from both spike trains

$C(t_k)$ is the coincidence value at time t for a spike k.

Python implementation of the SPIKE synchronization known as pyspike has been used for the analysis **(Kreuz et al., 2015; Mulansky and Kreuz, 2016).**

K-medoid Clustering

K-medoid is a partitional algorithm used to cluster data sets into different groups. In this method the aim is to group data into clusters such that their distance to the medoid of the cluster is minimized. The medoid selected for clustering is one of the data points. R implementation of the k-medoid clustering was used.

The analysis involving CMDS, spike synchrony and K-medoid clustering was done by Divye, a Masters student from Savitribai Phule Pune University.

Simulation

All network simulations were carried out using a fourth order Runge Kutta integration method. The time step used for simulation was 27µs. The input onset was set at 1000ms so as that the cells settle down to resting state. The input was provided for 6000ms and started to decay at 7000ms. The entire simulation was done for 8000ms. Simulations were performed using an in house developed open source C++ library called as '**in-silico'**. The in house '**in-silico**' utilizes boost library (odeint) for integrating the system of coupled differential equations. MATLAB was used to visualize and analyze data.

3.4 Results

3.4.1 Clustering mitral cell network using Newman Modularity Algorithm

Since odorant molecules are recognized by multiple ORNs and a particular odorant receptor can recognize many odorant molecules it has been proposed that odors are represented in a combinatorial manner (combinatorial coding scheme) **(Hallem and Carlson, 2006; Malnic et al., 1999)**. It has also been proposed that different odors activate different subnetworks of the olfactory bulb and hence we sought to understand how the network structure governs the dynamics. For this we first constructed a random subnetwork of 50 mitral cells using the WS model. As described in the previous chapter our simplified network consists of mitral cells inhibiting each other, hence our random network is a purely inhibitory network. To determine groups of neurons that will be maximally disconnected, the flipped version of the adjacency matrix was passed through the Newman modularity algorithm. The algorithm pulled out groups based on the edge density within and across the group. The indices of the neurons were then permuted on the original matrix according to the clusters obtained from the clustering algorithm. This rearrangement of the original adjacency matrix revealed block like structures with minimal within group connections (diagonal blocks of zero) and all the across group connections represented by 1's present on the off diagonal. Figure 3.3 outlines the procedure for the methodology used for finding such groups by us. A uniquely colored network has zero within group connections and all connections are across groups. Our final rearrangement of the adjacency matrix matches quite closely to such a uniquely colored network. The network used in this example had four groups which we have represented with four colors (red, blue, green and orange). The group sizes revealed by the algorithm shows that groups are of unequal sizes with red group consisting of 15 neurons, blue consisting of 14 neurons, green consisting of 11 neurons and orange consisting of 10 neurons.

We constructed several such random networks and used this algorithm to find out the sizes of the communities. We looked for only those groups whose size was greater than six as we defined this to be the threshold for being a meaningful group. Figure 3.4 shows the frequency of various group sizes. We found that the distribution of group sizes lied in the range 10-16 and thus the groups detected were mostly of similar size. The average size of the group was found to be 12. We constructed several such random networks and applied this algorithm to find their modularity (as shown in Figure 3.5).
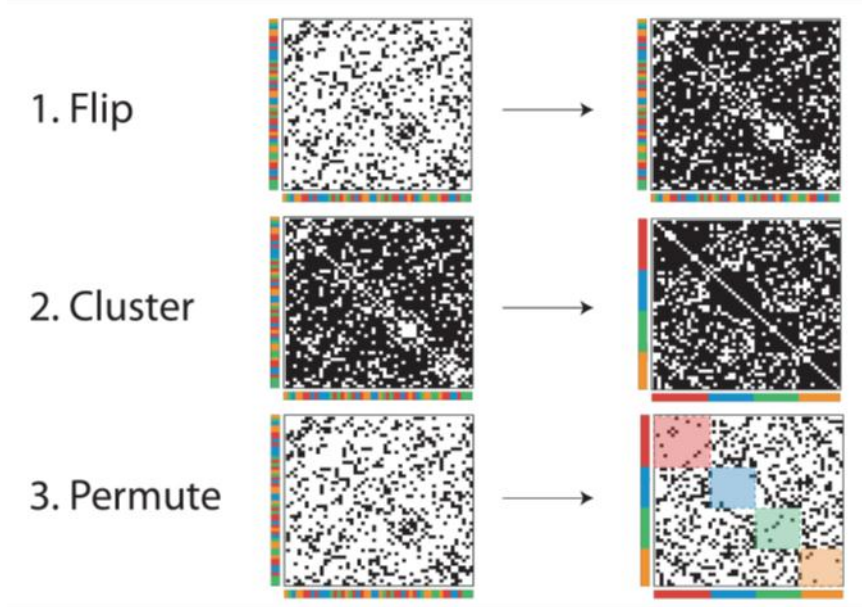
Figure 3.3 Clustering using Newman Algorithm

Adjacency matrix of a random network. A black dot (indicating 1 in the adjacency matrix) at the location (i,j) indicates that the ith neuron inhibits the jth neuron. In step 1, the adjacency matrix was transformed by converting the ones to zeros. The diagonal elements were not changed. In step 2, we used the Newman clustering algorithm to detect clusters of densely connected nodes in the flipped network. The nodes were rearranged such that those belonging to a cluster were put in adjacent rows/columns. The original (but permuted) adjacency matrix was obtained by switching back the ones to zeros and vice versa. This created diagonal blocks that had minimal connections and off-diagonal regions with a randomly distributed mix of ones and zeros.
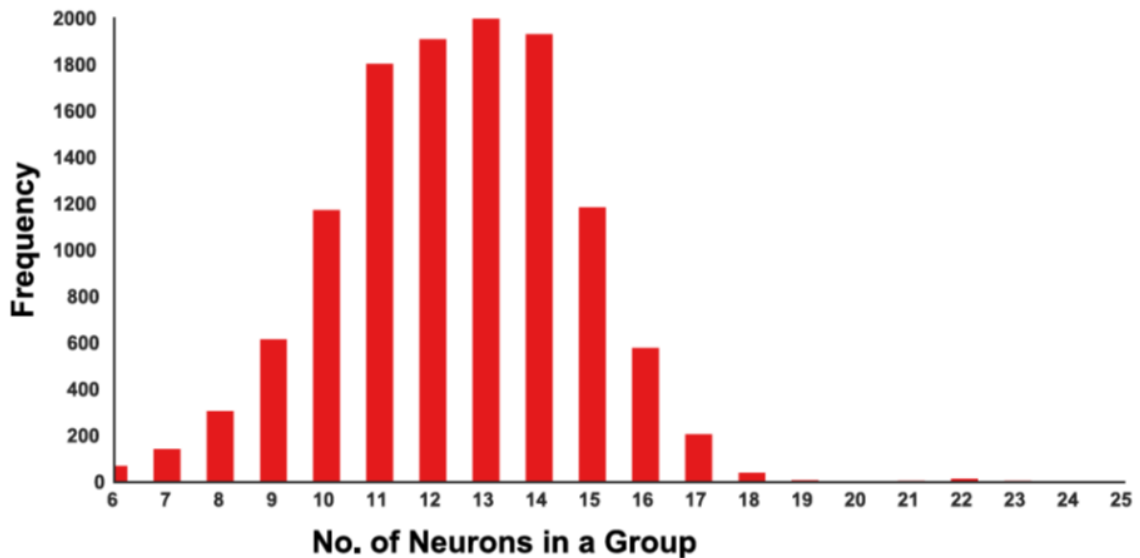
Figure 3.4 Distribution of group sizes upon clustering

Histogram showing the distribution of group sizes obtained on clustering different random networks. The average size of the groups is 12.

Figure 3.5 Clustering of few Random Networks using Newman Algorithm

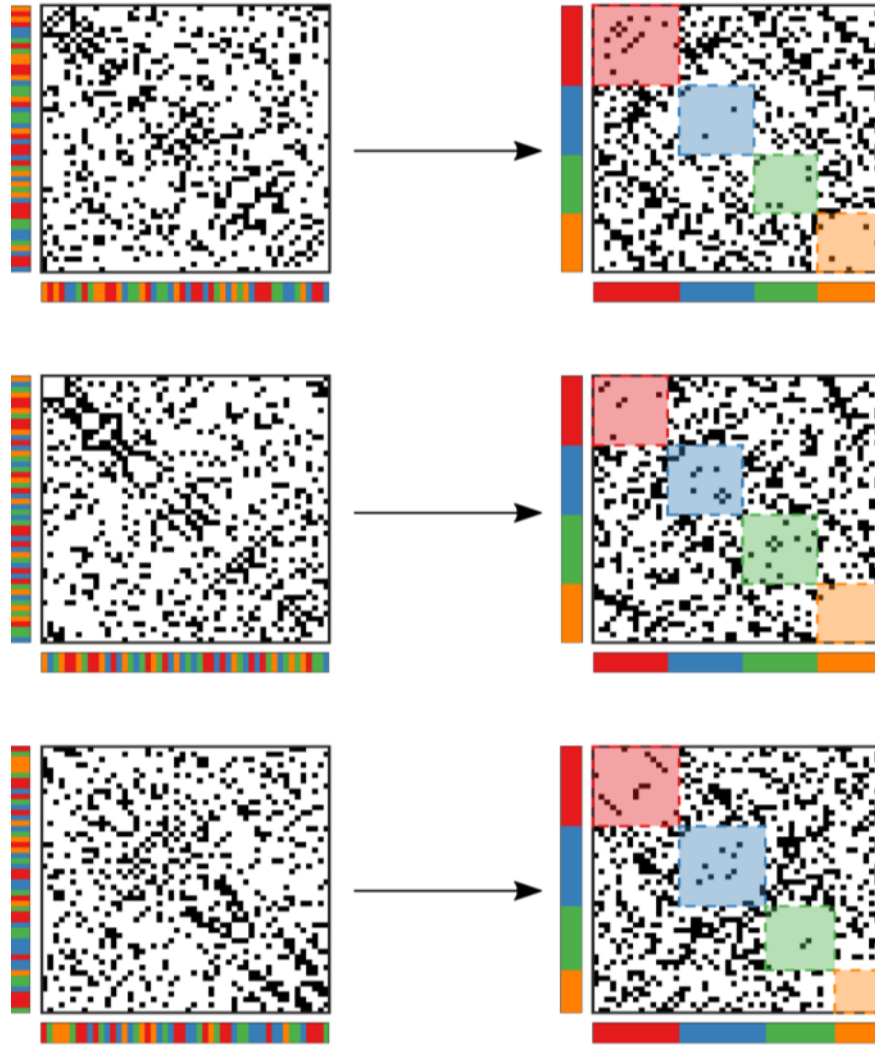Examples of few random networks that were clustered using the procedure outlined in Figure 3.3. The random networks shown here have a total of 4 distinct groups shown in different colors.

3.4.2 Using modularity algorithm and determining correlations in the dynamics

Assuming all neurons receive similar input and the network structure respects the groupings, neurons belonging to the same group will not compete amongst each other and spike synchronously, whereas neurons belonging to other groups will fire antagonistically and at different times. This antagonistic interaction leads to alternation in the firing patterns of different groups and constitutes a spatiotemporal pattern. Upon constructing the random network and finding its modularity, we asked whether we can detect the impression of the network in the dynamics. In other words, we looked for correlation in the dynamics with the groups found. We simulated different instances of random network by providing similar input to all the neurons in the random network. The system was given 1000ms to reach steady state, after which the stimulus was provided for 6000ms. The raster plot in Figure 3.6A shows the dynamics of the random network over 3700 milliseconds. The dynamics without the rearranging the network do not show any ordering or spatiotemporal pattern, however when we rearrange the neurons according to the groups the hidden correlations are revealed (Figure 3.6B). The neurons associated with the red color fire synchronously, so do the neurons associated with the blue, green and orange color. The neurons in the red, blue, green and orange groups alternate in their firing pattern. Such dynamics have been demonstrated already for uniquely colored networks **(Assisi et al., 2011)**. We calculated correlation coefficients for within group neurons and across the group neurons by convolving their activity with a square pulse (window =50ms).We compared these correlations, with the correlations obtained from a random clustering of the network. Correlations calculated based on the Newman clustering revealed the presence of groups as observed in the structure and we found the groups to be positively correlated among themselves and negatively correlated to the other groups. Correlations based on a random clustering showed no such group like structure (Figure 3.7). We simulated different instances of random networks and found that the algorithm was able to extract groups which showed positive correlations within the groups and negative correlations across the groups (Figure 3.8A). We simulated a particular random network across different noise trials. We found that these correlations persisted across different noise instances as the distribution of the negative and positive correlations were different from each other (Figure 3.8B).

Our methodology gives us different possible valid solutions for the system. These solutions correspond to distinct possible spatiotemporal patterns that the network can generate. The modularity places constraints on the number of distinct spatiotemporal patterns that can be

generated and gives an estimate on the capacity for encoding large number of different odor stimulus. The total number of distinct possible combinations generated is referred to as the Capacity(C) of the network. According to a previous work, for a system of N neurons the capacity is given by the following equation (N≥3) (**Rabinovich et al., 2001**):

$$C = \sum_{k=3}^{N} \binom{N}{k} (k-1)! = N! \sum_{k=3}^{N} \frac{1}{k(N-k)!}$$

In our case N can be considered to as the total number of distinct groups.

A)

B)
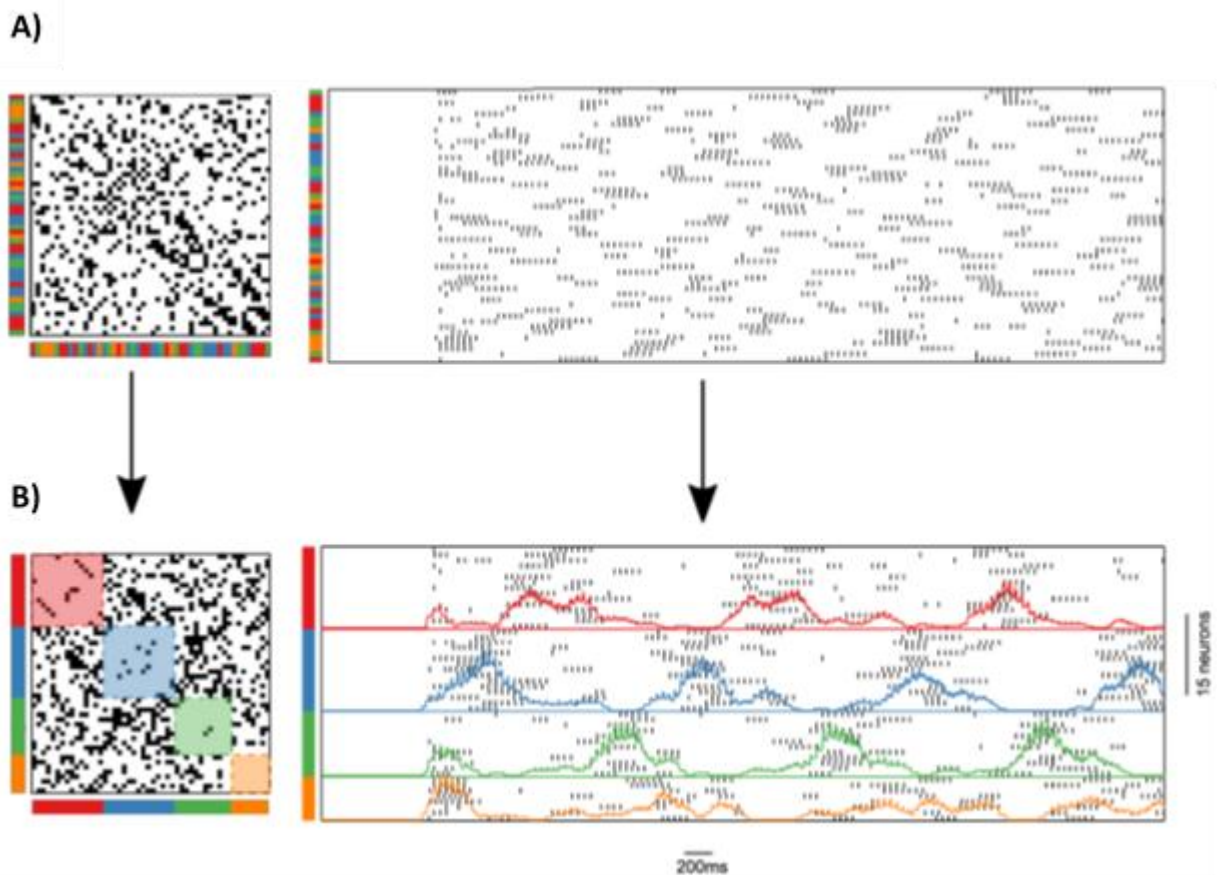
Figure 3.6 Dynamics of a random network

A random network of 50 neurons was simulated. The top left panel shows the connectivity/adjacency matrix of a random network. It is a 50 X 50 matrix with black dots showing connection between the neurons (entry value =1) and white showing no connection between the neurons (entry value=0). The colorbar indicates the coloring of the neurons in the network. The top raster plot shows the activity of this particular network. The bottom right is the rearranged connectivity matrix, upon coloring the graph reveals the block like structures. The bottom raster plot which is rearranged according to the block like structure reveals that the dynamics obey the coloring of the network. The raster is shown from 2500ms to 6200ms.
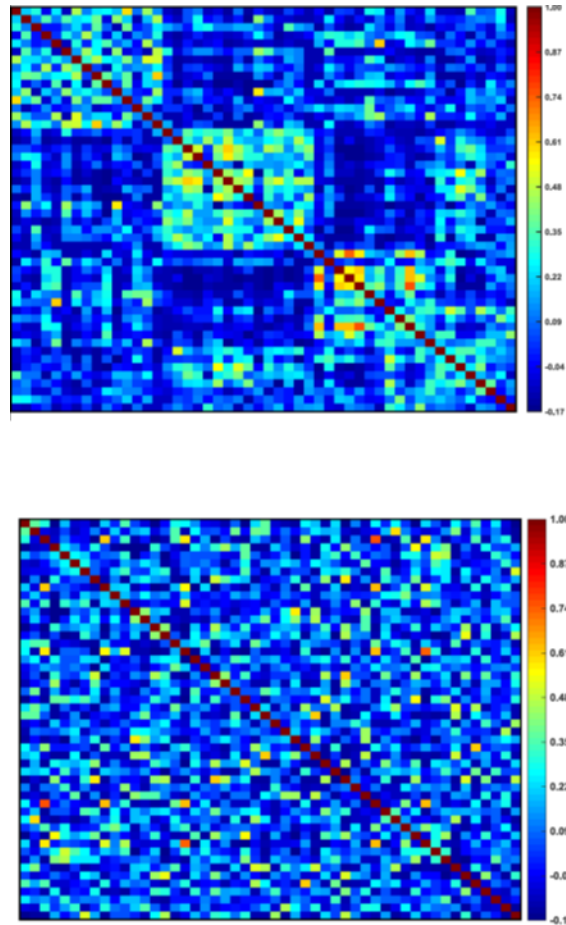
Figure 3.7 Correlation coefficient in the dynamics according to Newman clustering

Correlation coefficient for all pairwise neuron activity was calculated after convolving with a square pulse (windows=50ms). The plot shows the correlation coefficient with the ordering obtained from Newman Algorithm (top panel) and compared with correlation coefficient arranged according to a random clustering (bottom panel). Notice that a block like structure is observed in the top panel.
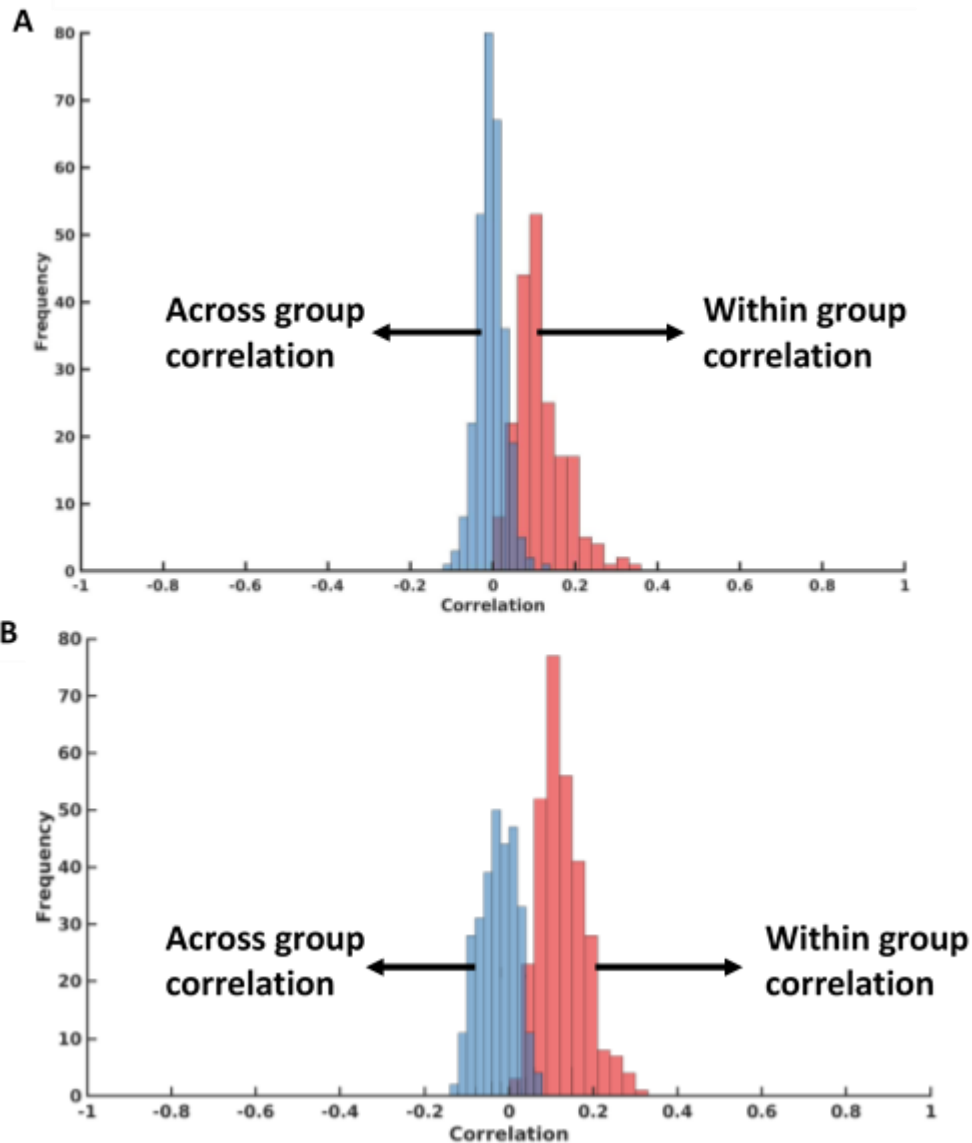
Figure 3.8 Distribution of correlations

Correlation coefficient was calculated, for within group and across group neuron spiking activity and the distribution of values is plotted as a histogram. The top histogram (A) shows the distribution for different instances of random networks. The below histogram (B) shows distribution for different noise trials of a particular random network.

3.4.3   Dynamics based Clustering

After finding that the hidden correlations in the dynamics are in agreement with the network structure, we asked whether we could cluster the neurons using their firing activity and if this would correlate with the clustering obtained from Newman algorithm. For this we recorded the spike times of each neuron in a vector. The spike time vector was then used to calculate pairwise

spike synchrony for all the neurons. Spike synchrony measure uses the spike times to calculate the average synchronization value of two spike trains. A value of 1 indicates that the two spike trains are fully synchronized and a value of 0 indicates they are not synchronized. Any intermediate value indicates that they were correlated at certain times and not correlated at other times during the stimulus duration. The idea behind using spike synchrony was that this measure could be used as a distance metric to cluster the neurons. The spike synchrony values were then used to build a dissimilarity matrix by subtracting them from 1. This was done so that a dissimilarity value of 0 means that the points are close together and 1 meant they are farther apart. Before clustering was performed, we first reduced the dimensionality of the system using Classical Multidimensional scaling. This was done for the purpose of visualizing the clusters. For our work, reducing the dimensionality to one dimension was found to be helpful. Clusters were then detected using k-medoid clustering method. The groups obtained through this method were used to replot the dynamics (shown as a raster plot) (Figure 3.9). The raster revealed the underlying antagonistic interactions between groups. Similar to the previous results, we looked for correlations within and across the groups and compared it with a random clustering. The correlations revealed the presence of a group like structure which is absent in the random clustering (Figure 3.10). We further sought to find the overlap between the groups obtained from Newman clustering and dynamics based clustering. Since the identities of the groups found through the dynamics based clustering are not known, we calculated the best overlap between Newman based clustering and structure based clustering. For this we found the overlap values with all possible combinations between Newman method and dynamics based method and the highest value was taken to be the overlap between both the methods for a particular random network. The overlap of 50 different instances of random network was calculated and the mean overlap was taken. Similarly, the best overlap between random clustering and dynamics based clustering for each network was done. The results (Figure 3.11) plotted as bar plot shows that dynamics based clustering had better overlap with the Newman based clustering method, thus further demonstrating that correlations found in the dynamics were governed by the structure.
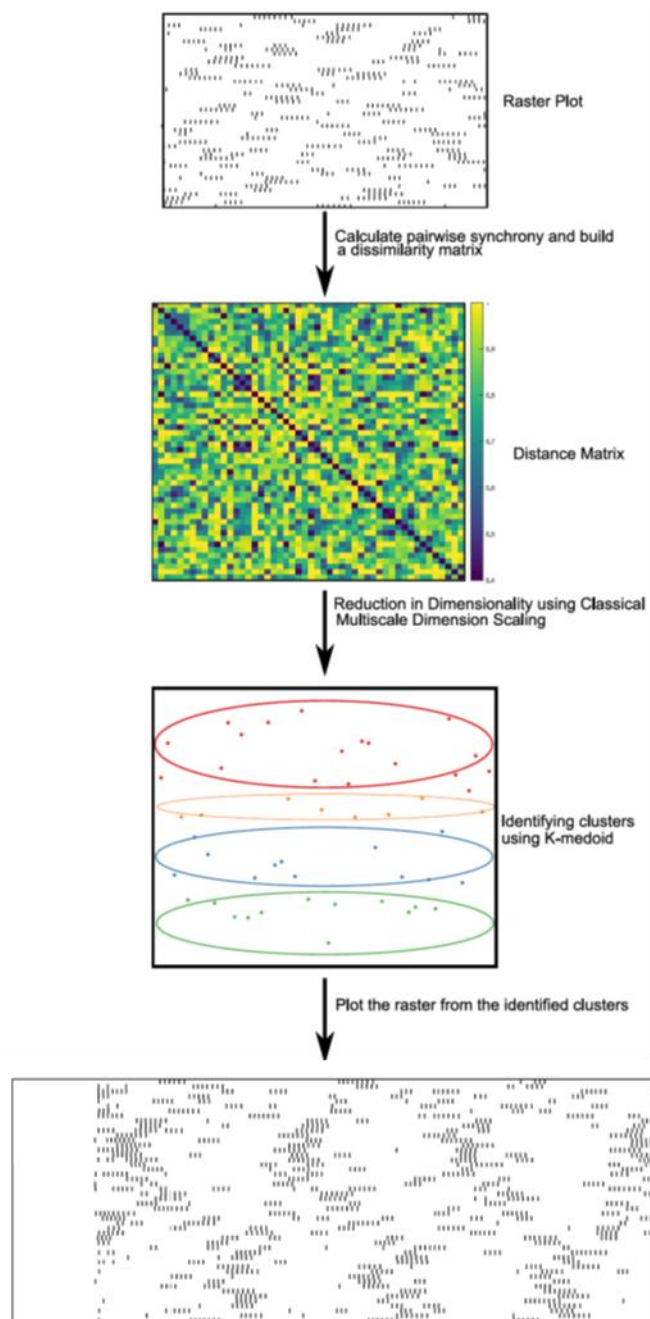
Figure 3.9 Approach to clustering using dynamics

Spike times are used to calculate pairwise spike synchrony between all the 50 neurons. This synchrony measure is then thresholded and is used to construct a distance matrix (second panel). The dimensionality of this system is then further reduced from 50 dimensions to 1 dimension using classical multidimensional scaling (third panel). This dimensionality reduction helps in identifying the clusters using k-medoid clustering method. Using the predicted clusters the dynamics are reordered to reveal the patterning (bottom panel).
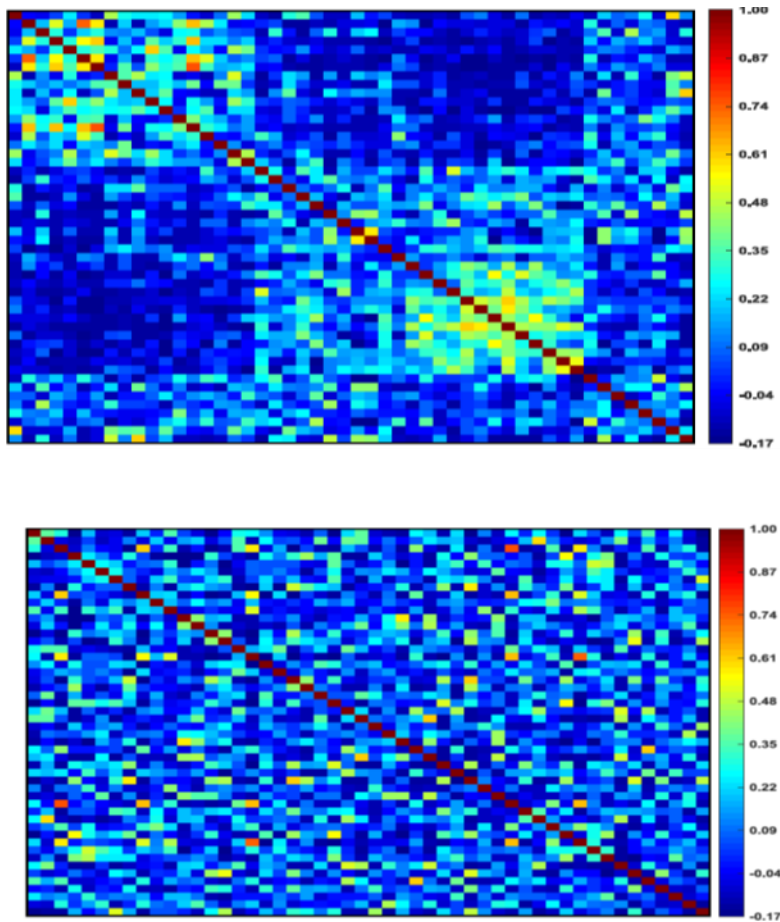
Figure 3.10 Correlation coefficient in the dynamics according to Dynamics based clustering

Correlation coefficient for all pairwise neuron activity was calculated after convolving with a square pulse (windows=50 ms). The plot shows the correlation coefficient with the ordering according to the clustering obtained from the dynamics based clustering (top panel) and compared with correlation coefficient arranged according to a random clustering (bottom panel). Notice that a block like structure is observed in the top panel.
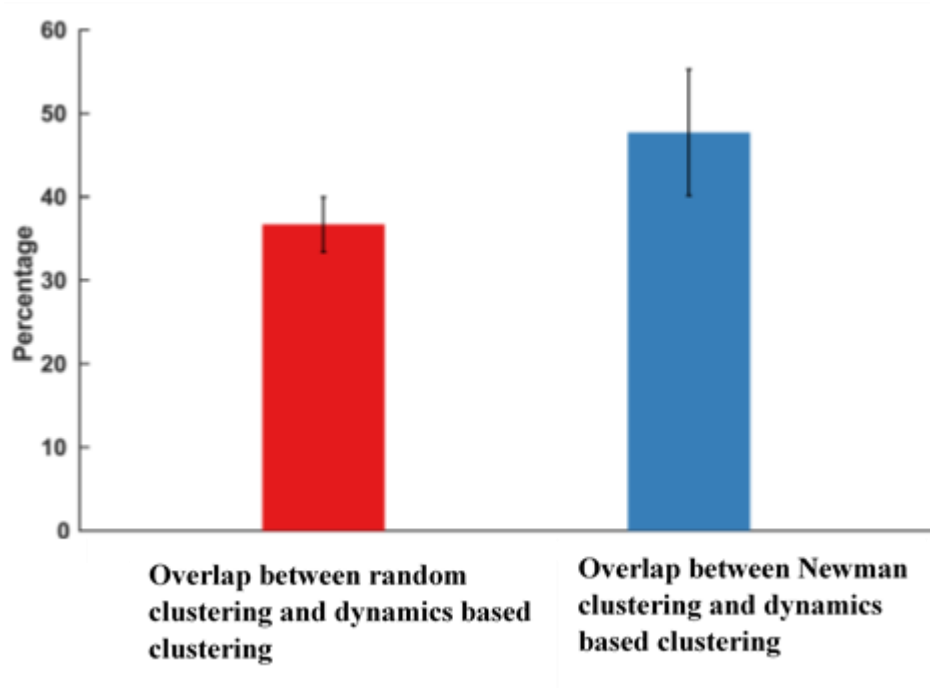
Figure 3.11 Comparison of overlap between groups predicted by Newman algorithm and Dynamics based clustering

The bar plot shows the percentage of overlap in the neurons predicted by the Newman algorithm and dynamics approach based algorithm, compared with the overlap between random clustering and dynamics based clustering.

3.5 Summary

The results above demonstrate how lateral inhibition among different groups of the mitral cells leads to synchronous firing of neurons associated with a particular group and they alternate in their activity with other groups. The rich spatiotemporal patterns generated by the olfactory system has been proposed to generate a large coding space for representation of olfactory stimulus (**Laurent, 2002**). In this work we have been able to demonstrate that structural properties of the mitral cell network and the resulting dynamics can be linked through modularity algorithm and it allows us to represent the dynamics of a high-dimensional complex system in lower dimensions, which is reduced to the minimal number of interacting groups. Asymmetries can stabilize some of the sequences generated by the olfactory bulb network in the network connectivity. Komarov et al. have shown that the network bursting pattern reflects the heterogeneities in the external stimulus (**Komarov and Bazhenov, 2016**). So input heterogeneities can also lead to particular stable sequences.

Although the work described here is for the circuitry of the olfactory bulb it can be generalized for the study of inhibitory networks involved in information processing in different brain regions.

Chapter 4: Reliability in Patterns

4.1 Introduction

Recordings of the mitral cells of zebrafish show that their activity evolves over time during stimulus presentation. The evolution of mitral cell activity helps in separating the initially similar patterns evoked by similar odors (**Friedrich and Laurent, 2001, 2004**). This separation of patterns is known as odor decorrelation and it helps the animal to discriminate odors from one another.

In the zebrafish, recordings of the electrical activity of mitral cells in response to different amino acids show that the patterns evoked are less variable upon presentation of the same odor across different trials (**Friedrich and Laurent, 2001, 2004).** These findings show that representations for a particular odor are reliable from trial to trial. Similarly, recordings of the locust antennal lobe show that odors elicit reliable responses of the PNs over different trials (**Laurent et al., 1996a; Perez-Orive et al., 2002; Wehr and Laurent, 1996**). Reliable spiking in response to repeated odor presentations is also observed in Drosophila PNs (**Bhandawat et al., 2007**). In rodents, optical imaging had revealed that same glomeruli were activated across trials in response to a particular odor (**Spors and Grinvald, 2002**).

Based on above studies, it can be inferred that the olfactory system is involved in achieving two goals, one is to discriminate between similar kinds of stimuli and second is to ensure reliable identification of the same odor presentation despite different noise variations. This is important since animals encounter odors under different environmental conditions and they should correctly identify the same odor with different noise background.

Network topology is one of the important factors that play a role in achieving reliability. Theoretical work with simple models and smaller networks within the framework of dynamical systems have shown that symmetries in the network topology can give rise to two distinct possibilities depending upon the coupling strength between the neurons. For weak coupling, the dynamical system has a global attractor in which all neurons get synchronized. If the coupling is strong then the system exhibits multi-stability, where only one neuron is active and others are quiescent and initial conditions determine which neuron remains active. However if asymmetry exists in the network the system enters a regime known as winner-less competition (WLC) –the system generates reliable sequential activity of neurons. In this regime the dynamics are robust to noise perturbations leading to reliability (**Rabinovich et al., 2001**).

Asymmetry in a network means that there are more connections going in one direction as compared to the other. In this chapter we explore whether such asymmetry in the network topology can bring about reliability in spatiotemporal patterns for larger and much higher dimensional mitral cell networks.

4.2 Methods

Mitral Cell Model and synapse model:

These are described in chapter 2

Network Structure:

A network consisting of 40 mitral cells were constructed having a unique coloring. Four groups of 10 neurons each were constructed in such a manner that neurons within a group did not make an inhibitory connection whereas they made inhibitory connections with the neurons belonging to other groups. This network's chromatic number was 4. Using the same network a unique sequence was embedded by making the connections asymmetric from group to another.

Entropy Measure:

This measure was used to calculate the reproducibility of sequences over trials

$$S_i = -\sum_j p_{i \to j} \log p_{i \to j}$$

Where S_i is the total entropy for a particular group i and p is the probability of transition of group i to group j **(Huerta and Rabinovich, 2004).**

Simulation

All network simulations were carried out using a fourth order Runge Kutta integration method. The time step used for simulation was 27μs. The input onset was set at 1000ms so as that the cells settle down to resting state. The input was provided for 6000ms and started to decay at 7000ms. The entire simulation was done for 8000ms. Simulations were performed using an in house developed open source C++ library called '**in-silico'**. The in house '**in-silico**' utilizes boost library (odeint) for integrating the system of coupled differential equations. MATLAB was used to visualize and analyze data.

4.3 Results

4.3.1 Asymmetry in the network produces reliable representations

We constructed a k-partite network consisting of 40 neurons which were divided into four groups of equal neurons. A k-partite network is a network which has no within group connections and all the connections lie across the groups. Figure 4.1A represents the adjacency matrix (A) of the k-partite network. The black dots indicate the presence of connections and for the k-partite they all lie on the off diagonal. The four groups are represented by four different colors because the k-partite network has a unique coloring. This network is full symmetric: if for every inhibitory connection going from node i to j there is a reciprocal connection going from j to i ($A_{ij} = A_{ji}$). This network was then simulated for 100 different noise trials. Upon simulation this network produced dynamics which were governed by the partitions of the network. Different trials of this network produced different patterns. As can be seen in Figure 4.1B, the patterns produced are different in each noise trial. Thus symmetric network produced dynamics which are unreliable across noise. We introduced an asymmetry in this network by having more synaptic connections in one direction as compared to the other direction (in the resulting adjacency matrix $A_{ij} \neq A_{ji}$) (Figure 4.2A). This asymmetry activated a particular sequence in the network. When this network was simulated for 100 trials and the activity pattern was plotted (raster plot) it was found that the same ordering of the groups occurred across different noise trials (Figure 4.2B).

We used entropy as a metric for measuring reliability. This measure uses probability of transition from one group to another and looks at how reliable these transitions are across noise trials. If there is successful transition from group A to group B across all noise trials then the entropy value of group A is zero. The probability of transition for a particular group was calculated taking into account 10 trials each, which allowed us to calculate the entropy over these 10 trials. Mean entropy value for the group was calculated by taking into account all the trials, by grouping the hundred total trials into groups of 10 each. This process was repeated similarly for all the other groups and a mean entropy value for the symmetric case was calculated by taking a mean of all the groups. A similar procedure was adopted for the asymmetric case. Figure 4.3 shows the entropy value of symmetric networks as compared to asymmetric networks. The asymmetric network has a highly reproducible transition among groups across noise trials hence its entropy value is close to zero whereas it is high for symmetric networks meaning the transitions are unreliable.
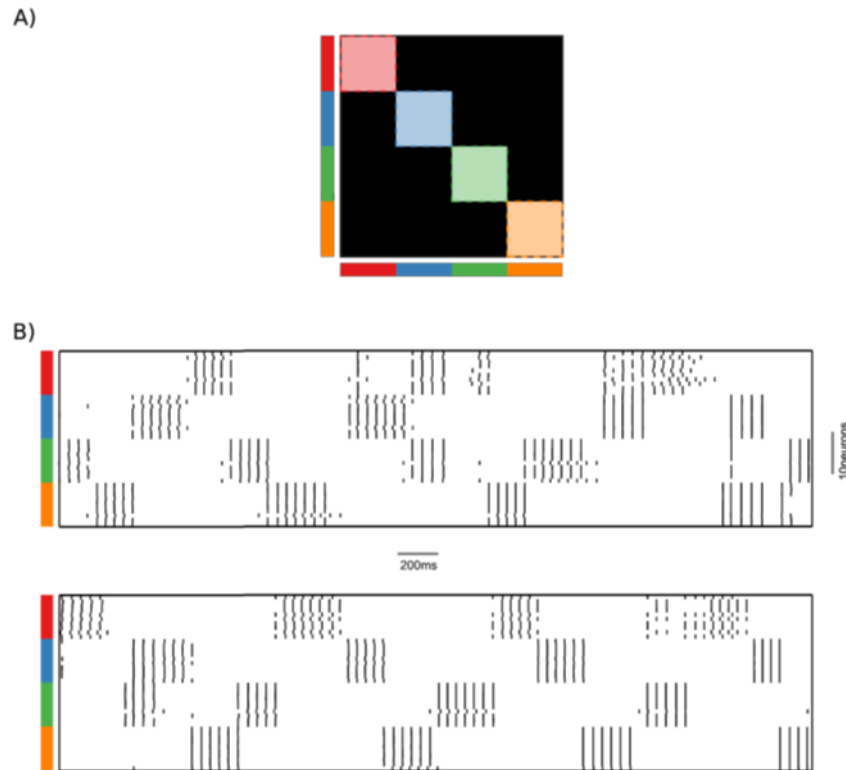
Figure 4.1 Symmetry in the network does not show reliability to noise

A) A perfectly symmetric k-partite network with four groups of equal number of neurons. All the off diagonal elements are black (entry=1) and the diagonal elements are colored according to the groups (entry=0).

B) Raster plot showing the dynamics of the k-partite network across noise trials. The top raster and the bottom raster are the dynamics across different noise trials of the same network. The dynamics reveal that different groups fire alternately but they do not fire reliably in the same manner across noise trials.
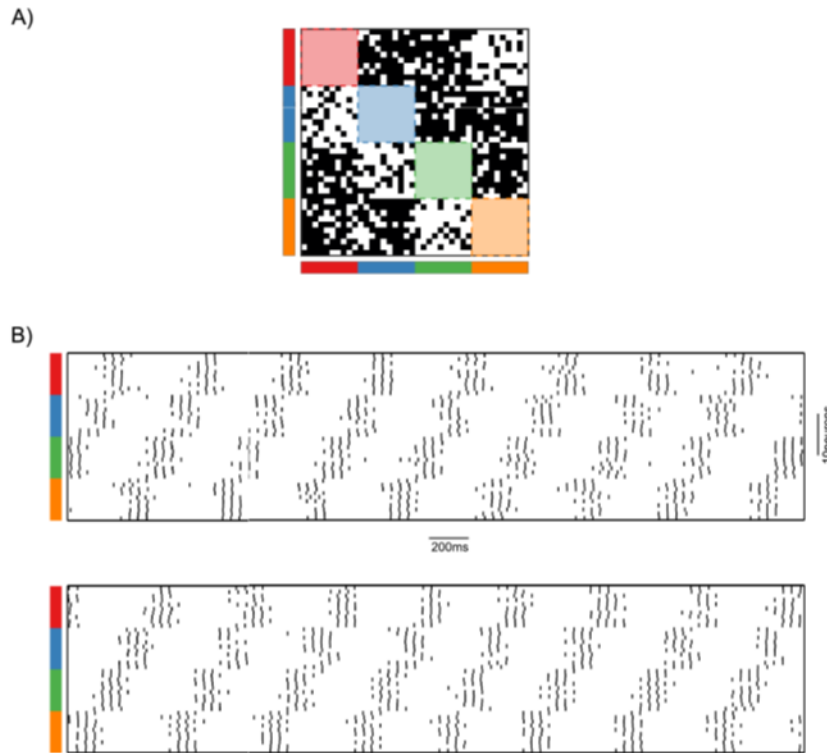
Figure 4.2 Asymmetry in the networks leads to reliability in ordering

A) Connectivity matrix of asymmetric network for a network with 4 groups consisting of equal number of neurons.

B) Raster plot showing the dynamics of the asymmetric network across noise trials. The top raster and the bottom raster are the dynamics across different noise trials of the same network. The dynamics reveal that the neurons of a particular group fire together and the firing of each group occurs in a sequential manner. The ordering of the groups is preserved across different noise trials.
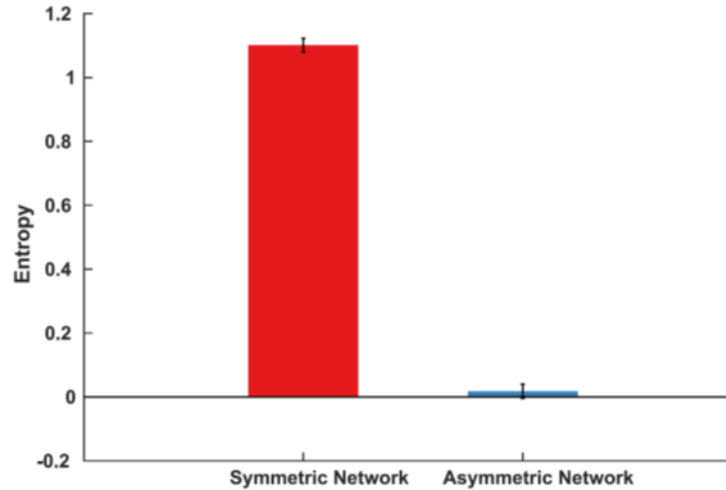
Figure 4.3 Reliability in dynamics across noise measured as entropy

The entropy measure calculates the reliability of one group transitioning to different groups. If firing of one group is followed by another group reliably then its entropy is close to zero.

The plot shows the mean entropy of all four groups sampled for 100 trials in groups of 10. Entropy for asymmetric network is close to zero whereas for symmetric networks the entropy is high.

4.4 Summary

4.4.1 Asymmetry in the random network

We see in our simulations that introducing asymmetry in the network coupling brings reliability in the ordering of patterns. Thus based on these results we reasoned that asymmetry in random networks can also produce reliable ordering. The random networks that we generated had symmetry in their connectivity (Figure 4.4). As shown in Figure 4.4, the total number of outgoing connections from red group to blue group is the same as from blue to red group. This is true for all the other groups. Asymmetry in the random networks can be introduced by deleting connections between two particular groups and redistributing it equally to the other remaining groups. We did this for one specific random network. As can be seen in Figure 4.5, introducing asymmetry by this method results in directionality in the network based on the outgoing connections, which are more in one direction and less in the other direction. Based on our simulations with k-partite networks, we predict that this network should result in the following sequence Red-> Orange->Green->Blue->Red and this sequence would be reliable. In the olfactory bulb, intrinsic asymmetries in the subnetwork could be present which could be activated by a particular odor, thus encoding a reliable representation for that odor.
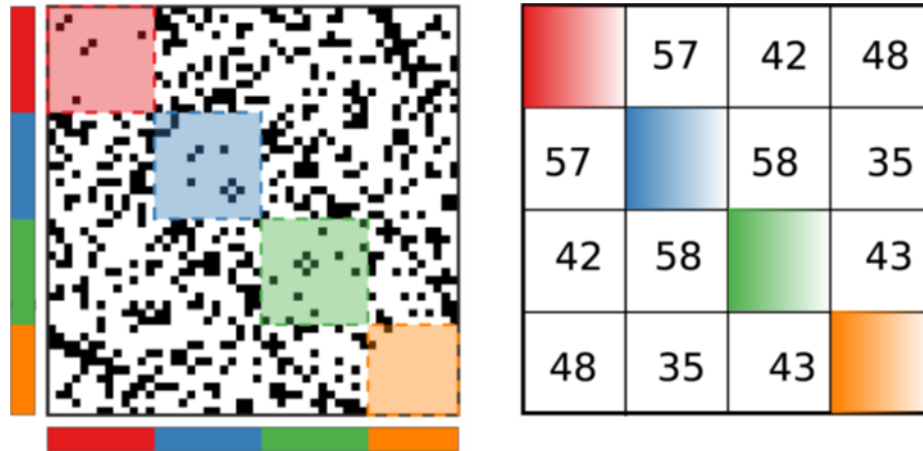
Figure 4.4 Adjacency matrix of a random network show the presence of symmetry in the network

A black dot indicates 1 whereas white is 0. The right shows the total number of inhibitory connections going from one group to the other. Since the total number of connections going from one to the group and vice versa are same hence the random networks are symmetric.
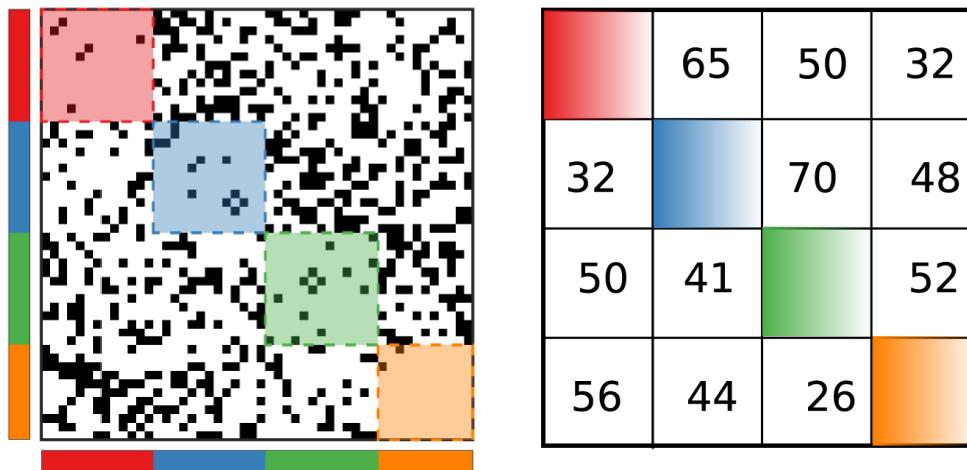
Figure 4.5 Adjacency matrix of a random network in which connections are deleted

The right matrix shows the total number of inhibitory connections going from one group to the other after deletion. There is an asymmetry in the network, as the number of connections going from one group and the number of connections it receives from that particular group are not same. This network should result in Red-> Orange->Green->Blue->Red sequence.

Chapter 5: Summary of findings

5.1 Discussion

In this study we have explored the relationship between the modularity of inhibitory networks and their dynamics with a view to understand how odor encoding occurs in the olfactory bulb. The objective was to study if an impression of the network structure can be detected in the dynamics of the network. Network modularity for inhibitory networks is defined as the group of neurons which are maximally disconnected from each other in the group but connect to neurons belonging to other groups. Gaining insights into the relationship between the structure and dynamics of a network is a complex task since the properties of the constituent neurons and synapses are non-linear and the system is high dimensional in nature. The main findings of the study were:

5.1.1 Hidden Correlations

We employed the Newman modularity algorithm to detect groups of neurons that were maximally disconnected from each other but made connections with neurons belonging to other groups. This algorithm helped us in finding such clusters of neurons in randomly generated networks. When dynamics were reordered based on the clustering obtained, we were able to extract hidden correlations between the dynamics and the structure of these random inhibitory networks. Simulating different networks showed that neurons belonging to a particular group fired together and neurons belonging to other groups fired at different times forming a spatiotemporal pattern. This kind of dynamics has been observed in neuronal networks that have reciprocal inhibitory connections, along with a slower time scale mechanism such as spike frequency adaptation (**Assisi et al., 2011**). Spike frequency adaptation involves a slow adaptation current, for example, the hyperpolarizing Ca^{2+} dependent potassium current in the insect antennal lobe PNs, which upon activation leads to cessation of neuronal activity after certain time. In our case it was the slow potassium current that allowed switching in the activity of neurons. We generated various instances of random networks and in all those networks the groups predicted by the modularity algorithm showed positive correlations in their spiking activity for within group dynamics and negative correlations across the groups. These correlations were found to be robust for changing noise perturbations. The methodology helped us in deducing all possible dynamics of the network provided they respect the modularity of the network. Thus, we are able to construct a link between the structural property of every inhibitory network and its dynamics. It has the added benefit of

describing a complex high dimensional system in a low dimensional space. The results obtained here are generic and not contingent upon the model used for random network generation. Random networks generated using the Erdos-Renyi model can also be clustered as shown in the Figure 5.1. We predict that the dynamics of this network would also show correlations with the structure.

As stated previously in Chapter 1, there are two theories regarding odor coding in the bulb: a combinatorial based encoding and spatiotemporal based encoding. Based on the combinatorial coding theory, studies carried out have shown that lateral inhibition in the bulb is involved in generating contrast enhancement **(Yokoi et al., 1995)**. This results in sharpening of representations and helps in discriminating similar odors. However, based on the spatiotemporal coding theory, studies show that the role of lateral inhibition is to generate sequential firing of synchronous ensembles of neurons **(Friedrich and Laurent, 2001)**. Our simulations support the role of lateral inhibition in generating spatiotemporal patterns which can lead to decorrelation of patterns evoked by similar odors **(Laurent, 2002)**. A caveat in our work is that we have reduced the olfactory bulb circuitry to a network of mitral cells coupled through lateral inhibition whereas in the bulb mitral cells are coupled to each other through granule cells which mediate reciprocal as well as lateral inhibition **(Shepherd and Greer, 2004)**.

A recent study has also shown that the heterogeneity in the external input is reflected in the inhibitory network dynamics **(Komarov and Bazhenov, 2016)**. The sequence of neuronal firing reflects the ranking (magnitude) of the external stimulus to the network. In our network we predict that a heterogeneous external input provided to each group would result in sequential activation of groups of neurons based on the ranking of the external stimulus.

In neuroscience there is a large interest in understanding how the network topology gives rise to dynamical behaviours such as synchronization. It has been found that synchronization of various brain regions form functionally coherent networks. Computational study done using realistic topology of cat corticocortical network has revealed that such dynamics are governed by the underlying network structure **(Zemanová et al., 2006)**. It has been found that brain at rest (when it is not performing any task) displays spontaneous dynamics with intermittent fluctuations. Resting state dynamics have been characterized by metabolic profile studies of the brain done using blood oxygen level dependent signal fluctuations (BOLD fMRI). These fMRI studies reveal functional connectivity between brain regions. Functional connectivity has been characterized by

quantities such as correlations, mutual information and covariance. These temporal correlations are also termed as resting state functional connectivity (rsFC). This temporal coherence between brain regions has provided evidence of the presence of robust resting state networks (RSNs). The most widely studied RSNs is the default mode network (DMN) **(Deco et al., 2011; Hutchison et al., 2013; Vincent et al., 2007)**. The DMN show decrease in their activity during the performance of a cognitive task as compared to baseline activity, whereas they are activated in the absence of the task. These DMNs are anticorrelated with regions that show task positive correlations **(Fox et al., 2005)**. Computational studies have found that the simulated dynamics of the rsFC matches up with the fMRI data and they are shaped by the underlying anatomical connectivity. The relationship between the rsFC and the structural connectivity has been found to be robust **(Honey et al., 2009)**. In our work also, we find correlations in the activity of neurons belonging to a group which are maximally disconnected from each other and the network topology gives rise to such dynamics. Our work is in contrast to the above studies since correlations (functional connectivity) mostly arise between regions that are anatomically connected.

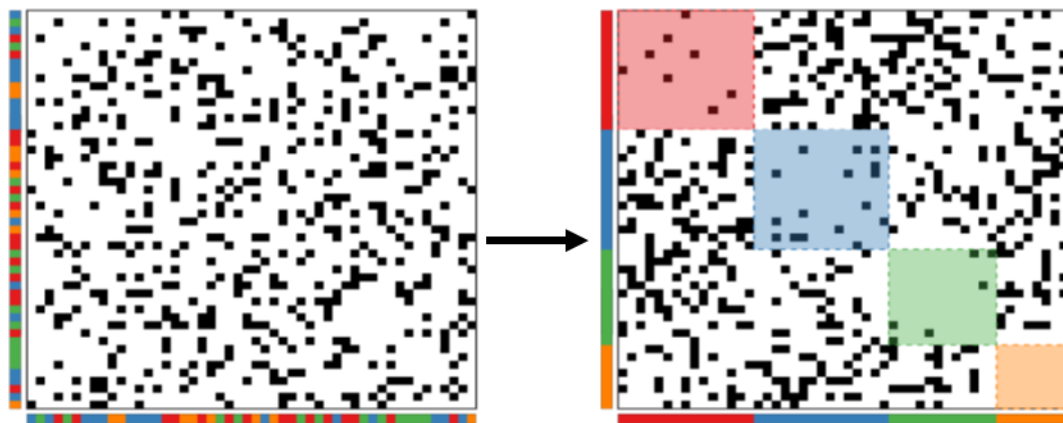**Figure 5.1 Random network generated through ER model**

Adjacency matrix of a random network generated using Erdos-Renyi model on the left. A black dot indicates 1 whereas white is 0. The random network was created using 50 nodes and the probability of connection is 0.2. The adjacency matrix of the rearranged network after clustering using Newman modularity shown on the right. The clustered network has four groups.

5.1.2 Asymmetries in the network lead to reliable ordering

Simulation of symmetric networks showed that the dynamics were unreliable across different noise trials, as each noise trial exhibited different temporal dynamics. Upon introduction of asymmetry in the connections we found that the dynamics of the network showed reliability across different noise perturbations.

Theoretical work using simplified models and smaller networks have illustrated how the spatiotemporal dynamics observed in the olfactory system can be explained through a competitive mechanism known as winnerless competition (WLC). According to WLC the spatiotemporal dynamics resemble heteroclinic orbits that connect unstable fixed points (known as saddle points). Each input stimulus is encoded by a different orbit, hence magnifying differences between the inputs over time. These orbits are robust and hence unperturbed by noise, thus ensuring trial to trial reliability. According to the study these orbits arise because of asymmetries in the network **(Afraimovich et al., 2004; Laurent et al., 2001; Rabinovich et al., 2001)**. In the context of olfactory encoding, the results imply that asymmetries in the bulb circuitry can stabilize representations for particular odors while making others unstable. Such asymmetries can arise due to learning mechanisms such as inhibitory facilitation. We hypothesize that the locus of such facilitation could be the granule-mitral cell GABAergic synapse. Computational study of the locust olfactory system has shown that inhibitory facilitation in the AL leads to coherent spiking activity in the PNs and introduces reliability **(Bazhenov et al., 2005)**.

Recent theoretical work has described that spatiotemporal dynamics can be conceptualized as trajectories (flows) on a low dimensional surface referred to as structured flow on manifolds (SFMs). The word structured implies "meaningful flow" in the state space and a manifold is a "low-dimensional" space which is specific to a certain behaviour. Usually high dimensional systems have effective low dimensional dynamics (functional activity). The SFM approach identifies the set of equations that defines this low dimensional manifold onto which the neuronal dynamics converge and evolve for the duration of an activity. Interestingly they find that SFMs arise because of asymmetries (deviations) in the network connectivity that leads to time scale separation in an otherwise invariant system. The SFMs introduced into the state space due to structural symmetry breaking also contributes to robustness in the system dynamics against noise perturbations **(Pillai and Jirsa, 2017)**.

5.2 Future directions

In this work the bulb network was modeled as an inhibitory network of mitral cells. However, the bulb contains inhibitory interneurons called granule cells which form reciprocal dendrodendritic synapses with the mitral cells. In the future explicit modeling of granule cells and the incorporation of excitatory synapses such as NMDA and AMPA from mitral cells to granule cells and GABAergic synapses from granule cells to mitral cells would help in understanding the computations occurring in the bulb circuitry. There is so far no evidence of granule cells being connected amongst each other.

Sniffing helps the rodents to explore the external environment. Sniffing occurs at a frequency of 4-12 Hz (**Deschenes et al., 2012; Welker, 1964**). Timing of neuronal firing relative to this sampling behavior carries information about the stimulus and is important in coding of odor representations (**Smear et al., 2011**). Studies show that odor evoked spiking activities of the tufted cells and mitral cells are phase locked with the sniff cycle. The tufted cells fire at the onset of the inhalation phase whereas the mitral cells fire during the inhalation-exhalation transition phase. These principal neurons also differ in their firing frequencies with tufted cells showing high frequency burst spikes whereas mitral cells showing lower-frequency burst spikes (**Fukunaga et al., 2012**). LFP recordings in the freely behaving rat showed the presence of two types of gamma oscillations. There was an early onset of fast gamma oscillations (65-100 Hz) and a late onset of slow gamma oscillations (40-65 Hz). These gamma oscillations were phase locked with the sniff cycle with the fast gamma occurring at early onset of inhalation (attributed to tufted cells) and slow gamma occurring at inhalation to exhalation transition (attributed to mitral cells) (**Manabe and Mori, 2013**). These findings showed that both the mitral and tufted cell circuitry generate distinct gamma oscillations in the olfactory bulb. A recent computational study has shown that theta oscillations induce reliable firing of the stellate cells in the medial entorhinal cortex. It has been demonstrated that theta oscillations create time windows such that only a particular group of interneurons respond to the external input, while others are suppressed. Theta oscillations lead to synchronization of stellate cells and they fired at a time when interneurons were hyperpolarized thus leading to reliability in the firing of both stellate cells and interneurons. Given the fact that theta oscillations can induce reliability it would be interesting to study if a similar mechanism exists with respect to sniff cycle (**Neru and Assisi, 2019).**

In psychophysical studies it has been found that bidirectional change in inhibition onto the mitral cells by granule cells affects odor discrimination times. For similar odor pairs it has been found that increasing inhibition leads to faster discrimination times, whereas decreasing inhibition leads to slower discrimination times **(Abraham et al., 2010)**. These studies suggest that inhibition plays a role in organizing spatiotemporal patterns of activity. Our results show that lateral inhibition is a key player in organizing these patterns. We speculate that, in these studies, it is lateral inhibition which is driving decorrelation of similar odors pairs as it aids in increasing the separation of patterns and this is achieved faster with increased inhibition. However, in addition to lateral inhibition, granule cells also mediate recurrent inhibition onto the mitral cells. These two forms of inhibition can play varying roles in the bulb.

References

Abraham, N.M., Egger, V., Shimshek, D.R., Renden, R., Fukunaga, I., Sprengel, R., Seeburg, P.H., Klugmann, M., Margrie, T.W., Schaefer, A.T.*, et al.* (2010). Synaptic inhibition in the olfactory bulb accelerates odor discrimination in mice. Neuron *65*, 399-411.

Abraham, N.M., Spors, H., Carleton, A., Margrie, T.W., Kuner, T., and Schaefer, A.T. (2004). Maintaining accuracy at the expense of speed: stimulus similarity defines odor discrimination time in mice. Neuron *44*, 865-876.

Ache, B.W., and Young, J.M. (2005). Olfaction: diverse species, conserved principles. Neuron *48*, 417-430.

Adrian, E.D. (1942). Olfactory reactions in the brain of the hedgehog. J Physiol *100*, 459-473.

Afraimovich, V.S., Rabinovich, M.I., and Varona, P. (2004). Heteroclinic contours in neural ensembles and the winnerless competition principle. International Journal of Bifurcation and Chaos *14*, 1195-1208.

Alioto, T.S., and Ngai, J. (2005). The odorant receptor repertoire of teleost fish. BMC Genomics *6*, 173.

Arbas, E.A., and Calabrese, R.L. (1987). Slow oscillations of membrane potential in interneurons that control heartbeat in the medicinal leech. J Neurosci *7*, 3953-3960.

Arenas, A., Diaz-Guilera, A., Kurths, J., Moreno, Y., and Zhou, C.S. (2008). Synchronization in complex networks. Phys Rep *469*, 93-153.

Assisi, C., Stopfer, M., and Bazhenov, M. (2011). Using the structure of inhibitory networks to unravel mechanisms of spatiotemporal patterning. Neuron *69*, 373-386.

Axel, R. (1995). The molecular logic of smell. Sci Am *273*, 154-159.

Balu, R., Larimer, P., and Strowbridge, B.W. (2004). Phasic stimuli evoke precisely timed spikes in intermittently discharging mitral cells. J Neurophysiol *92*, 743-753.

Bathellier, B., Lagier, S., Faure, P., and Lledo, P.M. (2006). Circuit properties generating gamma oscillations in a network model of the olfactory bulb. J Neurophysiol *95*, 2678-2691.

Bazhenov, M., Stopfer, M., Rabinovich, M., Huerta, R., Abarbanel, H.D., Sejnowski, T.J., and Laurent, G. (2001). Model of transient oscillatory synchronization in the locust antennal lobe. Neuron *30*, 553-567.

Bazhenov, M., Stopfer, M., Sejnowski, T.J., and Laurent, G. (2005). Fast odor learning improves reliability of odor responses in the locust antennal lobe. Neuron *46*, 483-492.

Benda, J., and Herz, A.V. (2003). A universal model for spike-frequency adaptation. Neural Comput *15*, 2523-2564.

Berkowicz, D.A., Trombley, P.Q., and Shepherd, G.M. (1994). Evidence for glutamate as the olfactory receptor cell neurotransmitter. J Neurophysiol *71*, 2557-2561.

Bhalla, U.S., and Bower, J.M. (1993). Exploring parameter space in detailed single neuron models: simulations of the mitral and granule cells of the olfactory bulb. J Neurophysiol *69*, 1948-1965.

Bhandawat, V., Olsen, S.R., Gouwens, N.W., Schlief, M.L., and Wilson, R.I. (2007). Sensory processing in the Drosophila antennal lobe increases reliability and separability of ensemble odor representations. Nat Neurosci *10*, 1474-1482.

Boyd, A.M., Sturgill, J.F., Poo, C., and Isaacson, J.S. (2012). Cortical feedback control of olfactory bulb circuits. Neuron *76*, 1161-1174.

Bozza, T., McGann, J.P., Mombaerts, P., and Wachowiak, M. (2004). In vivo imaging of neuronal activity by targeted expression of a genetically encoded probe in the mouse. Neuron *42*, 9-21.

Brea, J.N., Kay, L.M., and Kopell, N.J. (2009). Biophysical model for gamma rhythms in the olfactory bulb via subthreshold oscillations. Proc Natl Acad Sci U S A *106*, 21954-21959.

Bressler, S.L., and Freeman, W.J. (1980). Frequency analysis of olfactory system EEG in cat, rabbit, and rat. Electroencephalogr Clin Neurophysiol *50*, 19-24.

Brown, D.A., and Adams, P.R. (1980). Muscarinic suppression of a novel voltage-sensitive K+ current in a vertebrate neurone. Nature *283*, 673-676.

Buck, L., and Axel, R. (1991). A novel multigene family may encode odorant receptors: a molecular basis for odor recognition. Cell *65*, 175-187.

Buck, L.B. (1996). Information coding in the vertebrate olfactory system. Annu Rev Neurosci *19*, 517-544.

Bullmore, E., and Sporns, O. (2009). Complex brain networks: graph theoretical analysis of structural and functional systems. Nat Rev Neurosci *10*, 186-198.

Chen, W.R., and Shepherd, G.M. (1997). Membrane and synaptic properties of mitral cells in slices of rat olfactory bulb. Brain Res *745*, 189-196.

Chen, W.R., Xiong, W., and Shepherd, G.M. (2000). Analysis of relations between NMDA receptors and GABA release at olfactory bulb reciprocal synapses. Neuron *25*, 625-633.

Cleland, T.A., and Linster, C. (2005). Computation in the olfactory system. Chem Senses *30*, 801-813.

de Olmos, J., Hardy, H., and Heimer, L. (1978). The afferent connections of the main and the accessory olfactory bulb formations in the rat: an experimental HRP-study. J Comp Neurol *181*, 213-244.

Deco, G., Jirsa, V.K., and McIntosh, A.R. (2011). Emerging concepts for the dynamical organization of resting-state activity in the brain. Nat Rev Neurosci *12*, 43-56.

Deschenes, M., Moore, J., and Kleinfeld, D. (2012). Sniffing and whisking in rodents. Curr Opin Neurobiol *22*, 243-250.

Desmaisons, D., Vincent, J.D., and Lledo, P.M. (1999). Control of action potential timing by intrinsic subthreshold oscillations in olfactory bulb output neurons. J Neurosci *19*, 10727-10737.

Dickson, C.T., Magistretti, J., Shalinsky, M.H., Fransen, E., Hasselmo, M.E., and Alonso, A. (2000). Properties and role of I(h) in the pacing of subthreshold oscillations in entorhinal cortex layer II neurons. J Neurophysiol *83*, 2562-2579.

Eisthen, H.L. (2002). Why are olfactory systems of different animals so similar? Brain, behavior and evolution *59*, 273-293.

Firestein, S. (2001). How the olfactory system makes sense of scents. Nature *413*, 211-218.

Fleidervish, I.A., Friedman, A., and Gutnick, M.J. (1996). Slow inactivation of Na+ current and slow cumulative spike adaptation in mouse and guinea-pig neocortical neurones in slices. J Physiol *493 (Pt 1)*, 83-97.

Fortunato, S. (2010). Community detection in graphs. Phys Rep *486*, 75-174.

Fox, M.D., Snyder, A.Z., Vincent, J.L., Corbetta, M., Van Essen, D.C., and Raichle, M.E. (2005). The human brain is intrinsically organized into dynamic, anticorrelated functional networks. Proc Natl Acad Sci U S A *102*, 9673-9678.

Friedrich, R.W., and Korsching, S.I. (1997). Combinatorial and chemotopic odorant coding in the zebrafish olfactory bulb visualized by optical imaging. Neuron *18*, 737-752.

Friedrich, R.W., and Korsching, S.I. (1998). Chemotopic, combinatorial, and noncombinatorial odorant representations in the olfactory bulb revealed using a voltage-sensitive axon tracer. J Neurosci *18*, 9977-9988.

Friedrich, R.W., and Laurent, G. (2001). Dynamic optimization of odor representations by slow temporal patterning of mitral cell activity. Science *291*, 889-894.

Friedrich, R.W., and Laurent, G. (2004). Dynamics of olfactory bulb input and output activity during odor stimulation in zebrafish. J Neurophysiol *91*, 2658-2669.

Fukunaga, I., Berning, M., Kollo, M., Schmaltz, A., and Schaefer, A.T. (2012). Two distinct channels of olfactory bulb output. Neuron *75*, 320-329.

Gao, Y., and Strowbridge, B.W. (2009). Long-term plasticity of excitatory inputs to granule cells in the rat olfactory bulb. Nat Neurosci *12*, 731-733.

Girvan, M., and Newman, M.E.J. (2002). Community structure in social and biological networks. P Natl Acad Sci USA *99*, 7821-7826.

Go, Y., and Niimura, Y. (2008). Similar numbers but different repertoires of olfactory receptor genes in humans and chimpanzees. Mol Biol Evol *25*, 1897-1907.

Gschwend, O., Abraham, N.M., Lagier, S., Begnaud, F., Rodriguez, I., and Carleton, A. (2015). Neuronal pattern separation in the olfactory bulb improves odor discrimination learning. Nat Neurosci *18*, 1474-1482.

Gupta, P., Albeanu, D.F., and Bhalla, U.S. (2015). Olfactory bulb coding of odors, mixtures and sniffs is a linear sum of odor time profiles. Nat Neurosci *18*, 272-281.

Guthrie, K.M., Anderson, A.J., Leon, M., and Gall, C. (1993). Odor-induced increases in c-fos mRNA expression reveal an anatomical "unit" for odor processing in olfactory bulb. Proc Natl Acad Sci U S A *90*, 3329-3333.

Haberly, L.B., and Price, J.L. (1977). The axonal projection patterns of the mitral and tufted cells of the olfactory bulb in the rat. Brain Res *129*, 152-157.

Hallem, E.A., and Carlson, J.R. (2006). Coding of odors by a receptor repertoire. Cell *125*, 143-160.

Heinzel, H.G. (1988). Gastric mill activity in the lobster. I. Spontaneous modes of chewing. J Neurophysiol *59*, 528-550.

Hildebrand, J.G., and Shepherd, G.M. (1997). Mechanisms of olfactory discrimination: converging evidence for common principles across phyla. Annu Rev Neurosci *20*, 595-631.

Honey, C.J., Sporns, O., Cammoun, L., Gigandet, X., Thiran, J.P., Meuli, R., and Hagmann, P. (2009). Predicting human resting-state functional connectivity from structural connectivity. Proc Natl Acad Sci U S A *106*, 2035-2040.

Hu, A., Zhang, W., and Wang, Z. (2010). Functional feedback from mushroom bodies to antennal lobes in the Drosophila olfactory pathway. Proc Natl Acad Sci U S A *107*, 10262-10267.

Huerta, R., and Rabinovich, M. (2004). Reproducible sequence generation in random neural ensembles. Phys Rev Lett *93*, 238104.

Hutcheon, B., and Yarom, Y. (2000). Resonance, oscillation and the intrinsic frequency preferences of neurons. Trends Neurosci *23*, 216-222.

Hutchison, R.M., Womelsdorf, T., Allen, E.A., Bandettini, P.A., Calhoun, V.D., Corbetta, M., Della Penna, S., Duyn, J.H., Glover, G.H., Gonzalez-Castillo, J.*, et al.* (2013). Dynamic functional connectivity: Promise, issues, and interpretations. NeuroImage *80*, 360-378.

Jourdan, F., Duveau, A., Astic, L., and Holley, A. (1980). Spatial distribution of [14C]2-deoxyglucose uptake in the olfactory bulbs of rats stimulated with two different odours. Brain Res *188*, 139-154.

Kashiwadani, H., Sasaki, Y.F., Uchida, N., and Mori, K. (1999). Synchronized oscillatory discharges of mitral/tufted cells with different molecular receptive ranges in the rabbit olfactory bulb. J Neurophysiol *82*, 1786-1792.

Kernighan, B.W., and Lin, S. (1970). An Efficient Heuristic Procedure for Partitioning Graphs. Bell Labs Technical Journal *49*, 291-307.

Komarov, M., and Bazhenov, M. (2016). Linking dynamics of the inhibitory network to the input structure. J Comput Neurosci *41*, 367-391.

Kreuz, T., Mulansky, M., and Bozanic, N. (2015). SPIKY: a graphical user interface for monitoring spike train synchrony. J Neurophysiol *113*, 3432-3445.

Lagier, S., Carleton, A., and Lledo, P.M. (2004). Interplay between local GABAergic interneurons and relay neurons generates gamma oscillations in the rat olfactory bulb. J Neurosci *24*, 4382-4392.

Laurent, G. (2002). Olfactory network dynamics and the coding of multidimensional signals. Nat Rev Neurosci *3*, 884-895.

Laurent, G., and Davidowitz, H. (1994). Encoding of olfactory information with oscillating neural assemblies. Science *265*, 1872-1875.

Laurent, G., Stopfer, M., Friedrich, R.W., Rabinovich, M.I., Volkovskii, A., and Abarbanel, H.D. (2001). Odor encoding as an active, dynamical process: experiments, computation, and theory. Annu Rev Neurosci *24*, 263-297.

Laurent, G., Wehr, M., and Davidowitz, H. (1996a). Temporal representations of odors in an olfactory network. J Neurosci *16*, 3837-3847.

Laurent, G., Wehr, M., Macleod, K., Stopfer, M., Leitch, B., and Davidowitz, H. (1996b). Dynamic Encoding of Odors With Oscillating Neuronal Assemblies in the Locust Brain. The Biological bulletin *191*, 70-75.

Lowe, G., and Gold, G.H. (1993). Nonlinear amplification by calcium-dependent chloride channels in olfactory receptor cells. Nature *366*, 283-286.

MacLeod, K., and Laurent, G. (1996). Distinct mechanisms for synchronization and temporal patterning of odor-encoding neural assemblies. Science *274*, 976-979.

Madison, D.V., and Nicoll, R.A. (1984). Control of the repetitive discharge of rat CA 1 pyramidal neurones in vitro. J Physiol *354*, 319-331.

Malnic, B., Hirono, J., Sato, T., and Buck, L.B. (1999). Combinatorial receptor codes for odors. Cell *96*, 713-723.

Manabe, H., and Mori, K. (2013). Sniff rhythm-paced fast and slow gamma-oscillations in the olfactory bulb: relation to tufted and mitral cells and behavioral states. J Neurophysiol *110*, 1593-1599.

Marder, E. (1998). From biophysics to models of network function. Annu Rev Neurosci *21*, 25-45.

Marder, E., and Bucher, D. (2001). Central pattern generators and the control of rhythmic movements. Curr Biol *11*, R986-996.

Marder, E., and Bucher, D. (2007). Understanding circuit dynamics using the stomatogastric nervous system of lobsters and crabs. Annu Rev Physiol *69*, 291-316.

Marder, E., and Calabrese, R.L. (1996). Principles of rhythmic motor pattern generation. Physiol Rev *76*, 687-717.

Meister, M., and Bonhoeffer, T. (2001). Tuning and topography in an odor map on the rat olfactory bulb. J Neurosci *21*, 1351-1360.

Meredith, M. (1992). Neural circuit computation: complex patterns in the olfactory bulb. Brain Res Bull *29*, 111-117.

Miller, J.P., and Selverston, A.I. (1982). Mechanisms underlying pattern generation in lobster stomatogastric ganglion as determined by selective inactivation of identified neurons. IV. Network properties of pyloric system. J Neurophysiol *48*, 1416-1432.

Mombaerts, P. (1999). Molecular biology of odorant receptors in vertebrates. Annu Rev Neurosci *22*, 487-509.

Mori, K., and Manabe, H. (2014). Unique Characteristics of the Olfactory System. In The Olfactory System:From Odor Molecules to Motivational Behaviors, K. Mori, ed. (Tokyo: Springer Japan), pp. 1-18.

Mulansky, M., and Kreuz, T. (2016). PySpike - A Python library for analyzing spike train synchrony. SoftwareX *5*, 183-189.

Mulloney, B., and Selverston, A.I. (1974). Organization of Stomatogastric Ganglion of Spiny Lobster .1. Neurons Driving Lateral Teeth. J Comp Physiol *91*, 1-32.

Nagayama, S., Homma, R., and Imamura, F. (2014). Neuronal organization of olfactory bulb circuits. Front Neural Circuits *8*, 98.

Neru, A., and Assisi, C. (2019). Theta oscillations gate the transmission of reliable sequences in the medial entorhinal cortex. bioRxiv, 545822.

Neville, K.R., and Haberly, L.B. (2004). Olfactory Cortex. In Synaptic organization of the brain (New York,NY: Oxford University Press), pp. 415-454.

Newman, M.E. (2006). Modularity and community structure in networks. Proc Natl Acad Sci U S A *103*, 8577-8582.

Newman, M.E. (2010). Matrix Algorithms and Graph partitioning. In Networks : An Introduction (Oxford: Oxford University Press), pp. 345-382.

Newman, M.E., and Girvan, M. (2004). Finding and evaluating community structure in networks. Physical review E, Statistical, nonlinear, and soft matter physics *69*, 026113.

Newman, M.E.J. (2004). Detecting community structure in networks. The European Physical Journal B *38*, 321-330.

Perez-Orive, J., Mazor, O., Turner, G.C., Cassenaer, S., Wilson, R.I., and Laurent, G. (2002). Oscillations and sparsening of odor representations in the mushroom body. Science *297*, 359-365.

Pillai, A.S., and Jirsa, V.K. (2017). Symmetry Breaking in Space-Time Hierarchies Shapes Brain Dynamics and Behavior. Neuron *94*, 1010-1026.

Pinching, A.J., and Powell, T.P. (1971a). The neuron types of the glomerular layer of the olfactory bulb. J Cell Sci *9*, 305-345.

Pinching, A.J., and Powell, T.P. (1971b). The neuropil of the glomeruli of the olfactory bulb. J Cell Sci *9*, 347-377.

Pinching, A.J., and Powell, T.P. (1971c). The neuropil of the periglomerular region of the olfactory bulb. J Cell Sci *9*, 379-409.

Price, J.L. (1973). An autoradiographic study of complementary laminar patterns of termination of afferent fibers to the olfactory cortex. J Comp Neurol *150*, 87-108.

Rabinovich, M., Volkovskii, A., Lecanda, P., Huerta, R., Abarbanel, H.D., and Laurent, G. (2001). Dynamical encoding by networks of competing neuron groups: winnerless competition. Phys Rev Lett *87*, 068102.

Rabinovich, M.I., Varona, P., Selverston, A.I., and Abarbanel, H.D.I. (2006). Dynamical principles in neuroscience. Reviews of Modern Physics *78*, 1213-1265.

Raman, B., Joseph, J., Tang, J., and Stopfer, M. (2010). Temporally diverse firing patterns in olfactory receptor neurons underlie spatiotemporal neural codes for odors. J Neurosci *30*, 1994-2006.

Restrepo, D., Teeter, J.H., and Schild, D. (1996). Second messenger signaling in olfactory transduction. J Neurobiol *30*, 37-48.

Robertson, H.M., and Wanner, K.W. (2006). The chemoreceptor superfamily in the honey bee, Apis mellifera: expansion of the odorant, but not gustatory, receptor family. Genome Res *16*, 1395-1403.

Royet, J.P., Distel, H., Hudson, R., and Gervais, R. (1998). A re-estimation of the number of glomeruli and mitral cells in the olfactory bulb of rabbit. Brain Res *788*, 35-42.

Rubin, B.D., and Katz, L.C. (1999). Optical imaging of odorant representations in the mammalian olfactory bulb. Neuron *23*, 499-511.

Rubin, B.D., and Katz, L.C. (2001). Spatial coding of enantiomers in the rat olfactory bulb. Nat Neurosci *4*, 355-356.

Rubinov, M., and Sporns, O. (2010). Complex network measures of brain connectivity: uses and interpretations. Neuroimage *52*, 1059-1069.

Rybak, J., and Menzel, R. (1993). Anatomy of the mushroom bodies in the honey bee brain: the neuronal connections of the alpha-lobe. J Comp Neurol *334*, 444-465.

Satterlie, R.A. (1985). Reciprocal inhibition and postinhibitory rebound produce reverberation in a locomotor pattern generator. Science *229*, 402-404.

Schild, D. (1988). Principles of odor coding and a neural network for odor discrimination. Biophys J *54*, 1001-1011.

Schoppa, N.E. (2006). Synchronization of olfactory bulb mitral cells by precisely timed inhibitory inputs. Neuron *49*, 271-283.

Selverston, A.I., and Mulloney, B. (1974). Organization of Stomatogastric Ganglion of Spiny Lobster .2. Neurons Driving Medial Tooth. J Comp Physiol *91*, 33-51.

Sharp, F.R., Kauer, J.S., and Shepherd, G.M. (1975). Local sites of activity-related glucose metabolism in rat olfactory bulb during olfactory stimulation. Brain Res *98*, 596-600.

Shepherd, G.M., and Greer, C.A. (2004). Olfactory Bulb. In Synaptic organization of the brain (New York,NY: Oxford University Press), pp. 165-216.

Singer, W. (1999). Neuronal synchrony: a versatile code for the definition of relations? Neuron *24*, 49-65, 111-125.

Smear, M., Shusterman, R., O'Connor, R., Bozza, T., and Rinberg, D. (2011). Perception of sniff phase in mouse olfaction. Nature *479*, 397-400.

Sporns, O. (2013). Structure and function of complex brain networks. Dialogues in clinical neuroscience *15*, 247-262.

Spors, H., and Grinvald, A. (2002). Spatio-temporal dynamics of odor representations in the mammalian olfactory bulb. Neuron *34*, 301-315.

Stewart, W.B., Kauer, J.S., and Shepherd, G.M. (1979). Functional organization of rat olfactory bulb analysed by the 2-deoxyglucose method. J Comp Neurol *185*, 715-734.

Stopfer, M., Bhagavan, S., Smith, B.H., and Laurent, G. (1997). Impaired odour discrimination on desynchronization of odour-encoding neural assemblies. Nature *390*, 70-74.

Su, C.Y., Menuz, K., and Carlson, J.R. (2009). Olfactory perception: receptors, cells, and circuits. Cell *139*, 45-59.

Touhara, K., and Vosshall, L.B. (2009). Sensing odorants and pheromones with chemosensory receptors. Annu Rev Physiol *71*, 307-332.

van den Heuvel, M.P., and Sporns, O. (2013). Network hubs in the human brain. Trends Cogn Sci *17*, 683-696.

Vassar, R., Ngai, J., and Axel, R. (1993). Spatial segregation of odorant receptor expression in the mammalian olfactory epithelium. Cell *74*, 309-318.

Vincent, J.L., Patel, G.H., Fox, M.D., Snyder, A.Z., Baker, J.T., Van Essen, D.C., Zempel, J.M., Snyder, L.H., Corbetta, M., and Raichle, M.E. (2007). Intrinsic functional architecture in the anaesthetized monkey brain. Nature *447*, 83-86.

Wachowiak, M., and Cohen, L.B. (2001). Representation of odorants by receptor neuron input to the mouse olfactory bulb. Neuron *32*, 723-735.

Watts, D.J., and Strogatz, S.H. (1998). Collective dynamics of 'small-world' networks. Nature *393*, 440-442.

Wehr, M., and Laurent, G. (1996). Odour encoding by temporal sequences of firing in oscillating neural assemblies. Nature *384*, 162-166.

Welker, W.I. (1964). Analysis of Sniffing of the Albino Rat 1). Behaviour *22*, 223-244.

Wilson, R.I., and Laurent, G. (2005). Role of GABAergic inhibition in shaping odor-evoked spatiotemporal patterns in the Drosophila antennal lobe. J Neurosci *25*, 9069-9079.

Yamaguchi, M. (2014). Interneurons in the Olfactory Bulb:Roles in the Plasticity of Olfactory Information Processing. In The Olfactory System:From Odor Molecules to Motivational Behaviors, K. Mori, ed. (Tokyo: Springer Japan), pp. 97-132.

Yang, X., Renken, R., Hyder, F., Siddeek, M., Greer, C.A., Shepherd, G.M., and Shulman, R.G. (1998). Dynamic mapping at the laminar level of odor-elicited responses in rat olfactory bulb by functional MRI. Proc Natl Acad Sci U S A *95*, 7715-7720.

Yokoi, M., Mori, K., and Nakanishi, S. (1995). Refinement of odor molecule tuning by dendrodendritic synaptic inhibition in the olfactory bulb. Proc Natl Acad Sci U S A *92*, 3371-3375.

Zemanová, L., Zhou, C., and Kurths, J. (2006). Structural and functional clusters of complex brain networks. Physica D: Nonlinear Phenomena *224*, 202-212.

Zhang, X., and Firestein, S. (2002). The olfactory receptor gene superfamily of the mouse. Nat Neurosci *5*, 124-133.

ELSEVIER LICENSE
TERMS AND CONDITIONS

Jun 11, 2019

This Agreement between Shivik Garg ("You") and Elsevier ("Elsevier") consists of your license details and the terms and conditions provided by Elsevier and Copyright Clearance Center.

License Number	4605321048357
License date	Jun 10, 2019
Licensed Content Publisher	Elsevier
Licensed Content Publication	Neuron
Licensed Content Title	Analysis of Relations between NMDA Receptors and GABA Release at Olfactory Bulb Reciprocal Synapses
Licensed Content Author	Wei R. Chen,Wenhui Xiong,Gordon M. Shepherd
Licensed Content Date	Mar 1, 2000
Licensed Content Volume	25
Licensed Content Issue	3
Licensed Content Pages	9
Start Page	625
End Page	633
Type of Use	reuse in a thesis/dissertation
Portion	figures/tables/illustrations
Number of figures/tables/illustrations	1
Format	both print and electronic
Are you the author of this Elsevier article?	No
Will you be translating?	No
Original figure numbers	Fig 5 B)
Title of your thesis/dissertation	Dynamics of Inhibitory Networks in the Olfactory Bulb
Expected completion date	Sep 2019
Estimated size (number of pages)	90
Requestor Location	Mr. Shivik Garg B-212 Computational Neuroscience Lab IISER Pune Pune, Maharashtra 411008 India Attn: Mr. Shivik Garg
Publisher Tax ID	GB 494 6272 12
Total	0.00 USD
Terms and Conditions	

 Copyright Clearance Center

Back to view order details

Copy order

Print this page
Print terms & conditions
Print citation information
(What's this?)

Confirmation Number: 11822276
Order Date: 06/10/2019

Customer Information

Customer: Shivik Garg
Account Number: 3001466791
Organization: Shivik Garg
Email: shivik.garg@students.iiserpune.ac.in
Phone: +91 2025908421

Search order details by: Choose One ▼ [   ] Go

This is not an invoice

Order Details

Annual review of physiology

Billing Status:
N/A

Order detail ID:	71919725
ISSN:	1545-1585
Publication Type:	e-Journal
Volume:	
Issue:	
Start page:	
Publisher:	ANNUAL REVIEWS
Author/Editor:	American Physiological Society (1887-)

Permission Status: ✅ Granted

Permission type: Republish or display content
Type of use: Thesis/Dissertation
Order License Id: 4605331455965

Hide details

Requestor type	Academic institution
Format	Print, Electronic
Portion	image/photo
Number of images/photos requested	2
The requesting person/organization	Shivik Garg
Title or numeric reference of the portion(s)	Figure 4 a), Figure 6b)
Title of the article or chapter the portion is from	Understanding circuit dynamics using the stomatogastric nervous system of lobsters and crabs
Editor of portion(s)	NA
Author of portion(s)	Eve Marder, Dirk Bucher
Volume of serial or monograph	69
Page range of portion	291-316
Publication date of portion	2007